**Monograph:**

eprints@whiterose.ac.uk
https://eprints.whiterose.ac.uk/

# A Three Compartmental Model of the Hemodynamic Response and Oxygen Delivery to Brain

Y Zheng[#], D Johnston[#], J Berwick[#], D Chen[#], S A Billings[*], J E W Mayhew[#]

#Neural Imaging Research Unit, Dept Psychology
*Dept Automatic Control and Systems Engineering

# A Three-Compartment Model of the Hemodynamic Response and

# Oxygen Delivery to Brain

Ying Zheng[a], David Johnston[a], Jason Berwick[a], Danmei Chen[a], Steve Billings[b] and John

Mayhew[a]


[a] Department of Psychology, University of Sheffield, Sheffield S10 2TP

[b] Department of Automatic Control and Systems Engineering, University of Sheffield,

Mappin Street, Sheffield S1 3JD

**Keywords:** Three compartments; Hemodynamic model; Oxygen transport to tissue.

**Correspondence to:**


Dr. Ying Zheng

Department of Psychology,

University of Sheffield,

Sheffield S10 2TP

Tel. +44-114-222-6511

Fax. +44-114-276-6515

Email: ying.zheng@sheffield.ac.uk

## ABSTRACT

We describe a mathematical model linking changes in cerebral blood flow, blood volume and the blood oxygenation state in response to stimulation. The model has three compartments to take into account the fact that the cerebral blood flow and volume as measured concurrently using laser Doppler flowmetry and optical imaging spectroscopy have contributions from the arterial, capillary as well as the venous compartments of the vasculature. It is an extension to previous one-compartment hemodynamic models which assume that the measured blood volume changes are from the venous compartment only. An important assumption of the model is that the tissue oxygen concentration is a time varying state variable of the system and is driven by the changes in metabolic demand resulting from changes in neural activity. The model recognises the effects of the pre-capillary arteriolar oxygen perfusion (that is the saturation of the arterial compartment being less than unity). Simulations are used to explore the sensitivity of the model and to optimise the parameters for experimental data. We conclude that the three-compartment model was better than the one-compartment model at capturing the hemodynamics of the response to changes in neural activation following stimulation.

# INTRODUCTION

The mathematical modelling of the hemodynamic response is an important part of the research in understanding brain function in human neuroscience. There are, in the literature, many mathematical models of the coupling between the hemodynamic responses such as cerebral blood flow, blood volume and blood oxygenation state to the underlying neural activity or cerebral metabolic rate of oxygen ($CMRO_2$). We will classify these models into two groups: steady state models, and dynamic models. Steady state models are concerned only with magnitude changes, whereas dynamic models take into account the transient characteristics as well as the steady state behaviour, hence are typically in the form of differential equations with respect to time. Once the transient characteristics are settled, the coupling between the input and output of a dynamic model describes their steady state relationship.

An influential steady state model of oxygen delivery to brain was presented by Buxton and Frank (Buxton and Frank, 1997). They used the diffusion equation to describe the oxygen loss along the capillary bed at steady state, (i.e., the partial temporal derivatives are zero,) and thus modelled the oxygen extraction fraction (OEF) from the capillary as a function of the normalised cerebral blood flow (CBF) based on the assumptions that tissue oxygen tension was zero and that blood oxygen concentration decreased exponentially along the capillary. A simple steady state nonlinear relationship between the normalised CBF and the normalised $CMRO_2$ was obtained and the model required large changes in CBF to support small changes in $CMRO_2$.

3

Hudetz (Hudetz, 1999) and Mintun et al. (Mintun et al., 2001) modelled the radial and axial gradients of oxygen tension in tissue surrounding a single capillary. The oxygen diffusion equation was then solved numerically for absolute $CMRO_2$ given absolute CBF. Both models used the assumption of linear decrease of blood oxygen concentration down the capillary and predicted a proportional relationship between oxygen delivery and utilisation.

Another steady state model of oxygen diffusion along the capillary was developed by Gjedde et al. (Gjedde et al., 1999) and Vafaee and Gjedde (Vafaee and Gjedde, 2000). Again the model related absolute $CMRO_2$ to absolute CBF as opposed to the normalised quantities used by Buxton and Frank. A parameter related to oxygen diffusion capacity was included, whereas in Buxton and Frank's model this parameter was assumed constant and thus eliminated during normalisation. The model assumptions included negligible tissue oxygen tension and linear decrease of oxygen along the capillary. The model was applied to positron emission tomography (PET) data and explained the increase in $CMRO_2$ as the combined effect of increased CBF and increased oxygen diffusion capacity in the region of activation. Other similar steady state models were presented by Hyder et al. (Hyder et al., 1998) and Hayashi et al. (Hayashi et al., 2003).

As the methods for measuring hemodynamic responses became more sophisticated with good time resolution, in particular as the functional magnetic resonance imaging (fMRI) technique was increasingly used as a means of inferring changes in neural activity,

dynamic modelling of the hemodynamic responses became increasingly important, as it could be used to uncover the neural signal which underlies the blood oxygen level dependent (BOLD) signal as measured by fMRI. One of the first dynamic models linking the hemodynamic responses to neural activity was developed by Friston et al. (Friston et al., 2000). They used (i) the Balloon/Windkessel model ((Buxton et al., 1998), (Mandeville et al., 1999b)) which was a dynamic model linking normalised cerebral blood volume (CBV) to normalised CBF in the venous compartment, (ii) a second order linear dynamic system linking normalised CBF to stimulation, (iii) a conservation equation for the normalised deoxy-hemoglobin in the venous compartment, and (iv) the steady state relationship between the oxygen extraction fraction (OEF) and normalised CBF derived by Buxton and Frank (Buxton and Frank, 1997). These combined to produce a fourth order nonlinear dynamic system linking the normalised deoxy-hemoglobin (Hbr) in the venous compartment to stimulation. Finally a static nonlinear function was used (Buxton et al., 1998) to link the normalised Hbr and CBV to the BOLD signal.

The above model was extended by Zheng et al. (Zheng et al., 2002) by considering the oxygen diffusion equation including both the spatial and temporal partial derivatives, thus incorporating dynamics in the OEF and the capillary oxygen concentration. It also assumed a non-zero tissue oxygen tension that was related to an additional state variable. The result was a nonlinear dynamic model with seven state variables most of which were normalised quantities. The model was used to fit optical imaging spectroscopy (OIS) data

5

from a brief stimulation paradigm and was found to produce physiologically plausible model parameters.

Instead of using normalised quantities, Valabregue et al. (Valabregue et al., 2003) developed a dynamic model using absolute quantities for the hemodynamic responses, similar to the steady state model of Vafaee and Gjedde (Vafaee and Gjedde, 2000). The model made full use of the oxygen diffusion equation, including non-zero tissue oxygen concentration. Hill's equation was used and the dynamic equations were solved numerically to yield time series for $CMRO_2$ as well as venous Hbr in response to changes in CBF. It also examined the effects of the assumption of exponential decay of oxygen along the capillary, as used by Buxton and Frank and applied in the dynamic models by Friston et al. and Zheng et al. Other dynamic models developed include those by Aubert and Costalat (Aubert and Costalat, 2002)and Hathout et al. (Hathout et al., 1999).

Most, if not all, of the existing hemodynamic models assume either explicitly or tacitly that the measured CBF, CBV and BOLD signals originate from the venous compartment. Although the major contribution of the BOLD signal comes from the deoxy-hemoglobin which is primarily in the veins, the CBF and CBV measurements obtained via laser Doppler flowmetry (LDF) and OIS are likely to come from the arterial, capillary and venous compartments. The adequate interpretation of the BOLD signal will depend on an appropriate hemodynamic model taking into account the hemodynamic changes in all three compartments. It is for this purpose that we developed the three-compartment

6

hemodynamic model presented in this paper. It is an extension to the one-compartment model (Zheng et al., 2002).

The theoretical framework of the three-compartment model will be presented in the next section. The sensitivity of the model output to the model parameters will be studied through simulations, and the model will be fitted to experimental data obtained from LDF and OIS. Both the simulation environment and the experimental procedures will be given in the Method section. The results will be compared to that obtained using the one-compartment model. We show that there are significant differences between the predictions of the two models.

**THEORY**

This section introduces the mathematical equations used for the three-compartment (3C) model and discusses the appropriate partitioning of the hemodynamic measurements. We will denote absolute quantities by capital letters and normalised quantities by lower case letters, e.g., $f = F/F_0$ and $v = V/V_0$ represent the normalised CBF and CBV respectively, and the subscript "0" denotes the baseline value. Furthermore the subscripts "$a$", "$c$" and "$v$" denote the arterial, capillary and venous compartments respectively.

**Partition of blood flow**

The time series of the normalised blood flow $f_{tot}$, as measured by LDF, is a mixture of blood flow through the three compartments. Under steady state conditions, blood flow

into and out of all three compartments is the same. During transient periods, if the volume of a compartment changes, then the flow out of that compartment will differ from that entering into the compartment. Throughout this paper we will assume that there are stimulus induced blood volume changes in both the arterial and the venous compartments, but that the blood volume in the capillary compartment remains constant, in particular there is no the capillary recruitment or dilation. This implies that CBF outflow from the arterial compartment is equal to the CBF inflow to the venous compartment at all times. Thus we write $f_{tot}$ as a weighted sum of the three components:

$$f_{tot} = w_a f_{a,in} + w_c f_c + w_v f_{v,out}, \qquad w_a + w_c + w_v = 1 \qquad (1)$$

where $f_{a,in}$, $f_c$ and $f_{v,out}$ are the normalised CBF entering the arterial compartment, through the capillary compartment and out of the venous compartment respectively. The weighting factors $w_a$, $w_c$ and $w_v$ for the three compartments sum up to unity. The model is insensitive to the choice of the weightings (simulation results not shown) due to the fact that $f_{a,in}$, $f_c$ and $f_{v,out}$ are very similar time courses, each downstream flow being a slightly delayed version of the one upstream. In our application, we assumed that $w_a = w_c = w_v = 1/3$. An alternative approach would be to link the weighting factors for flow to the proportions assigned to the baseline blood volumes in the three compartments.

## Compartmental modelling

*Dynamic relationships in the arterial compartment*

The 3C model assumes that the arterial oxygen saturation $S_a$ can be less than unity. The implication is that oxygen diffusion may occur from arterioles to its surrounding tissue

8

((Vovenko, 1999), (Berwick et al., 2004)). However the oxygen diffusion rate through the wall of the arterial compartment is smaller than that through the capillary bed, and hence is not modelled explicitly here.

We have also considered changes in the arterial oxygen saturation and its inclusion in the 3C model. However when fitted to our experimental data, the magnitude and subsequent effect of arterial saturation changes was extremely small for most of our data sets. We will therefore assume throughout this paper that the arterial oxygen saturation stays constant.

The dynamic relationship between the normalised arterial CBF and CBV can be modelled using the modified Windkessle/Balloon model (Kong et al., 2004) which used an additional state variable to model the delayed compliance. This modified version has been demonstrated to capture the mismatch between the changes in CBF and CBV during the return-to-baseline phase of the time courses. Hence the flow-volume relationship of the arterial compartment is given by

$$\tau_a \dot{v}_a = f_{a,in} - f_c, \quad f_c = \frac{v_a^{\alpha_a + \beta_a}}{\kappa_a}$$
$$\tau_{\kappa_a} \dot{\kappa}_a = v_a^{\beta_a} - \kappa_a$$
(2)

where $f_{a,in}$ is the normalised blood flow into the arterial compartment and is the input of the arterial compartment model. The state variable $\kappa_a$ models the delayed compliance in the arterial compartment and is in normalised units with initial condition of 1. $\tau_a$ and $\tau_{\kappa_a}$ are the arterial transit time and the arterial compliance time constant respectively. The

well-known Grubb's exponent (Grubb et al., 1974) is given by $1/\alpha_a$ because at steady state, the above model becomes $f_c = v_a^{\alpha_a}$. The parameter $\beta_a$ models the degree of compliance in the compartment. If $\beta_a = 0$, there is no compliance in the compartment and the above model becomes the original Balloon model.

As the arterial saturation is constant, it is easy to show that the normalised deoxy-hemoglobin ($q_a = Q_a/Q_{a0}$) is given by $q_a = v_a$.

*Dynamic relationships in the capillary compartment*

The dynamic model describing the oxygen transport to tissue remains the same as the one-compartment (1C) model (Zheng et al., 2002) with three state variables: the oxygen extraction fraction (OEF) denoted by $E$, the mean capillary concentration $\overline{C_B}$ and the tissue to arterial end of capillary oxygen tension ratio $g$. The model was derived based on the work of Buxton and Frank (Buxton and Frank, 1997) and Hyder et al. (Hyder et al., 1998) with the important modification that oxygen concentration in tissue was nonzero. In the model, the rate of oxygen diffusion from capillary bed into tissue was assumed to be proportional to the *difference* in oxygen concentration between plasma and tissue, i.e.,

$$\frac{dC_B(x,t)}{dt} = -k\big(C_P(x,t) - C_t(t)\big) \tag{3}$$

where $x$ was the spatial coordinate along the capillary, $t$ was the time, $C_B(x,t)$ was the total oxygen concentration in blood as a function of space and time, $C_P(x,t)$ was the oxygen concentration in plasma as a function of space and time, $C_t(t)$ was the spatial

10

average oxygen concentration in tissue as a function of time only, and $k$ was a constant depending on the permeability and surface area of capillary exchange, amongst other factors. The 3C model has used the same capillary model, but has substituted the oxygen concentration $C$ by the normalised quantity: oxygen saturation $S$. This is because the measurements we obtain from OIS experiments are not oxygen concentration, but blood oxygen saturation. This modification does not affect the validity of the equations. Thus the capillary model can be written as

$$\frac{\varphi}{f_c}\dot{E} = -E + (1-g)\left(1 - \left(1 - \frac{E_0}{1-g_0}\right)^{\frac{1}{f_c}}\right) \tag{4a}$$

$$\frac{\varphi}{f_c}\dot{\bar{S}}_c = -\bar{S}_c - \frac{S_a E}{\ln\left(1 - \frac{E}{1-g}\right)} + S_a g \tag{4b}$$

$$\frac{\rho}{E_0}\dot{g} = \left(\frac{\bar{S}_c - gS_a}{\bar{S}_{c0} - g_0 S_{a0}} - 1\right) - M \tag{4c}$$

where $f_c$ is the normalised blood flow into the capillary compartment and $M$ represents the metabolic demand as a time series. Both are inputs to the capillary compartment model. The parameter $\varphi$ relates to the capillary transit time and the parameter $\rho$ is the lumped constant of the original term $J\dfrac{V_{tis}rT}{V_{cap}}$ in the 1C model where $V_{cap}$ and $V_{tis}$ are the blood volume in capillary and tissue respectively, $r$ is the ratio of oxygen concentration in plasma to that in blood and is assumed constant (Buxton and Frank, 1997). Our simulation (Zheng et al., 2002) showed that this is a reasonable assumption and avoids the complication of using the full Hill's equation. $T$ is the mean capillary transit time, and $J$ is an unknown scaling constant (Zheng et al., 2002). The replacement of the above

11

term by the single parameter $\rho$ is for notational clarity. In our previous work, we adjusted the scaling factor $J$ to fit the 1C model to our data. In the current work, we will optimise the parameter $\rho$ which reflects the time constant of the tissue oxygen concentration.

In the 1C model, the metabolic demand $M$ was modelled as the stimulus input scaled by a constant. This usually resulted in a very sharp initial decrease in the tissue oxygen concentration variable $g$. In the current model, the change in metabolic demand was modelled as a linear second order system driven by the stimulus input. In Laplace transform notation this can be written as

$$M(s) = \frac{K_M}{\dfrac{s^2}{\omega^2} + \dfrac{2\zeta s}{\omega} + 1} U(s) \tag{5}$$

where $s$ is the Laplace operator, $U(s)$ and $M(s)$ are the Laplace transforms of the stimulus and the metabolic demand time series respectively. We chose the damping ratio $\zeta = 1$ and the undamped natural frequency $\omega = 8$ rad/s. This ensures that the metabolic demand has no over- or undershoot during the stimulus onset and cessation phases of its time course. The gain of the system $(K_M)$ will then be optimised to indicate the magnitude of the changes in metabolic demand.

The oxygen saturation along the capillary decreases from $S_a$ at the arterial end to $S_{v,in}$ at the venous end. From the definition of the OEF we obtain:

$$S_{v,in} = S_a(1-E) \tag{6}$$

12

*Dynamic relationships in the venous compartment*

In the venous compartment, the blood volume as well as oxygen saturation of the compartment will change due to changes in neural activity. We model the dynamic relationship between the normalised CBF and CBV in the similar way as that of the arterial compartment. Hence the flow-volume relationship of the venous compartment is given by

$$\tau_v \dot{v}_v = f_c - f_{v,out}, \quad f_{v,out} = \frac{v_v^{\alpha_v + \beta_v}}{\kappa_v}$$
$$\tau_{\kappa_{v_v}} \dot{\kappa}_v = v_v^{\beta_v} - \kappa_v \tag{7}$$

Again the driving input of the venous compartment model is the normalised flow $f_c$ into the compartment. The state variable $\kappa_v$ models the delayed compliance, and $\tau_v$ and $\tau_{\kappa_v}$ are the venous transit time and the time constant for the delayed compliance respectively. $\alpha_v$ is the inverse Grubb's exponent of the venous compartment, and $\beta_v$ is the exponent such that at steady state $\kappa_v = v_v^{\beta_v}$.

Due to changes in neural activity, the saturation in the venous compartment will change. Assuming instantaneous mixing, the saturation inside the venous compartment $S_v$ is homogenous and is different from the oxygen saturation $S_{v,in}$ of the incoming blood during transient periods. By using the mass balance equation, it is easy to show that the normalised deoxy-hemoglobin $q_v$ in the venous compartment is related to the normalised CBF and saturation by

13

$$\tau_v \dot{q}_v = f_c \frac{1 - S_{v,in}}{1 - S_{v0}} - f_{v,out} \frac{q_v}{v_v} \, . \tag{8}$$

The saturation $S_v$ of the venous compartment is given by

$$S_v = 1 - (1 - S_{v0}) \frac{q_v}{v_v} \, . \tag{9}$$

where from Eqn.(6), the baseline venous oxygen saturation is given by $S_{v0} = S_a (1 - E_0)$.

**Blood volume partitioning**

The 3C model assumes that the time series CBV as measured by OIS is the sum of blood volumes in the arterial, capillary and venous compartments, i.e., $V_{tot} = V_a + V_c + V_v$, although changes in blood volume due to changes in neural activity are assumed to occur only in the arterial and the venous compartments, i.e., $\Delta V_{tot} = \Delta V_a + \Delta V_v$ where the prefix $\Delta$ denotes changes.

*Baseline blood volume*

The blood volume contained in the whole venous system is about 65% of the total blood volume, whereas the capillary system contains only 5% of the total blood volume. The rest of the blood is contained in the heart and the arterial system. However as our measurements were taken in cerebral brain regions while avoiding large blood vessels, the above proportions are inappropriate. In this paper we assumed that in the baseline condition, the volume fractions $p_a$, $p_c$ and $p_v$ in the arterial, capillary and venous compartments are 25%, 15% and 60% respectively. These are in accordance with the

existing literature (Duong and Kim, 2000). The effect of the baseline blood volume proportions will be shown in the result section.

*Changes in blood volume*

The total normalised CBV time series $v_{tot}$ can be written in terms of the normalised arterial and venous CBV time series $v_a$ and $v_v$ as

$$v_{tot} = \frac{V_a + V_c + V_v}{V_{tot0}} = p_a v_a + p_c + p_v v_v \tag{10}$$

assuming zero CBV changes in the capillary compartment (i.e. $v_c = 1$). Clearly from the above equation, there is no unique way of partitioning $v_{tot}$ into $v_a$ and $v_v$. As we have two models Eqn.s (2) and (7) linking $v_a$ and $v_v$ to the normalised CBF respectively, and we can measure the normalised CBF ($f_{tot}$) via LDF, the partitioning of $v_{tot}$ can be achieved by optimisation using the models. It seems that one could optimise the eight parameters ($\tau_a, \tau_{\kappa_a}, \alpha_a, \beta_a, \tau_v, \tau_{\kappa_v}, \alpha_v, \beta_v$) to provide the best fit to the OIS measurement $v_{tot}$ given the LDF measurement $f_{tot}$. However it is important to realise that there are steady state constraints which have implications on the dependence of the parameters.

The first steady state constraint stems from the Grubb's relationship which is a steady state relationship. For the 3C model at steady state, CBF is the same for all compartments, thus the Grubb's relationship implies that

$$v_{a,ss}^{\alpha_a} = f_{ss} = v_{v,ss}^{\alpha_v} \tag{11}$$

where the subscript "ss" denotes steady state. This shows that $\alpha_a$ and $\alpha_v$ are linked by the steady state changes in CBV in the arterial and venous compartments. For small percentage changes in CBV, the above equation can be expressed in the linearised form:

$$\alpha_a \frac{\Delta V_{a,ss}}{V_{a,0}} = \alpha_v \frac{\Delta V_{v,ss}}{V_{v,0}} \tag{12}$$

The second steady state constraint was based on the study by Lee et al. (Lee et al., 2001) who measured the total CBV and CBF changes, as well as the arterial CBV and total CBF changes. They found that *at steady state* the fractional CBV change in the arteries was 2.5 times the fractional change of the total CBV obtained assuming a CBF baseline of 58mℓ.min$^{-1}$.100g$^{-1}$ at which $V_{a0} \cong 0.25 V_{tot0}$. We will use the following notation

$$r_a = \frac{\Delta V_{a,ss}/V_{a0}}{\Delta V_{tot,ss}/V_{tot0}}, \qquad r_v = \frac{\Delta V_{v,ss}/V_{v0}}{\Delta V_{tot,ss}/V_{tot0}} \tag{13}$$

to denote the steady state arterial and venous fractional CBV to total CBV changes respectively. Based on the assumption of no capillary recruitment or dilation, $\Delta V_{tot,ss} = \Delta V_{a,ss} + \Delta V_{v,ss}$, thus the two ratios $r_a$ and $r_v$ are related by

$$r_a p_a + r_v p_v = 1 \tag{14}$$

It is easy to see from Eqn.s (12) and (13) that the parameters $\alpha_a$ and $\alpha_v$ and the fractional volume ratios $r_a$ and $r_v$ are algebraically linked by the equation

$$\alpha_a r_a = \alpha_v r_v \tag{15}$$

This means that if one has prior knowledge of the ratio $r_a$ and the baseline blood volume partitions, then the ratio $r_v$ can be calculated (using Eqn.(14)) and the Grubb's exponents in the arterial and the venous compartments are tightly coupled by Eqn.(15). Only one of

16

them should be optimised to maintain a sensible steady state relationship between blood volume changes. In our current work, we chose to optimise the parameter $\alpha_a$.

*Compliance and transit times*

There are also dynamic characteristics which are well-known to be significantly different between the arterial and the venous compartments. One of these characteristics is the vascular compliance property which is considered to be the main physiological mechanism for the observation that blood volume returns to baseline much slower than blood flow. As the arterial blood vessel is more elastic than that of the venous, one would expect that the arterial CBV returns to baseline much quicker than the venous CBV. In terms of the model parameters, this implies that $\beta_a$ should be much smaller than $\beta_v$. However there is no existing literature on the precise relationship between the two parameters. We found that if the two parameters were optimised as independent parameters, it was possible to have $\beta_a \gg \beta_v$ such that the delayed compliance observed in the measured CBV ($v_{tot}$) would be attributed to be largely present in the arterial compartment. To avoid this, we set the parameter $\beta_a = 0$ to force the delayed compliance in $v_{tot}$ to be accounted for only by the venous compartment, therefore only the parameter $\beta_v$ was optimised. This also implies the elimination of the time constant $\tau_{\kappa_a}$.

To further reduce confounding of the parameters, we selected the transit times $\tau_a$ and $\tau_v$ using existing literature for the arterial and venous compartments so that the other only unknown parameter to be optimised was the time constant $\tau_{\kappa_v}$.

*Optimisation strategy*

Thus our partitioning strategy for the time series $v_{tot}$ is as follows.

(i) Select the weightings for the normalised flow $w_a$, $w_c$ and $w_v$ and the baseline blood volume fractions $p_a$, $p_c$ and $p_v$.

(ii) Select the parameter $r_a$. This will enable the parameter $r_v$ to be calculated from Eqn. (13).

(iii) Select the transit times $\tau_a$ and $\tau_v$, and set $\beta_a = 0$.

(iv) Define the cost function

$$L_1\left(\alpha_a, \beta_v, \tau_{\kappa_v}\right) = \sum \left(v_{tot} - \hat{v}_{tot}\right)^2 \tag{16}$$

where $\hat{v}_{tot} = p_a \hat{v}_a + p_c + p_v \hat{v}_v$.

(v) Optimise the parameters $\alpha_a$, $\beta_v$ and $\tau_{\kappa_v}$ to minimise the above cost function.

The time series $\hat{v}_a$ and $\hat{v}_v$ can be obtained by solving the following equations simultaneously:

$$\tau_a \dot{\hat{v}}_a = f_{a,in} - \hat{v}_a^{\alpha_a}$$

$$\tau_v \dot{\hat{v}}_v = \hat{v}_a^{\alpha_a} - \frac{\hat{v}_v^{\alpha_v + \beta_v}}{\kappa_v}$$

$$\tau_{\kappa_v} \dot{\kappa}_v = \hat{v}_v^{\beta_v} - \kappa_v$$

$$f_{a,in} = \frac{1}{w_a}\left(f_{tot} - w_c f_c - w_v f_v\right) = \frac{1}{w_a}\left(f_{tot} - w_c \hat{v}_a^{\alpha_a} - w_v \frac{\hat{v}_v^{\alpha_v + \beta_v}}{\kappa_v}\right)$$

where the parameter $\alpha_v$ is calculated using the constraint Eqn.(15). The time series $\hat{v}_a$ and $\hat{v}_v$ thus obtained satisfy the steady state constraints. Furthermore the delayed compliance in $v_{tot}$ is captured by the dynamic model of the venous compartment.

**Summary**

The major differences between the 1C and the 3C models are that in the 3C model the arterial compartment is modelled by a dynamic equation allowing the arterial CBV to change due to changes in CBF, and that the arterial saturation can be less than unity. The dynamic equations modelling the capillary compartment are the same in the two models. The partitioning of total blood flow, volume, saturation and deoxy-hemoglobin into the three compartments are shown in Table 1.

In this paper we do not deal with the dynamic relationship between stimulation, neural activity and the changes in CBF as it is independent of the architecture of the 3C model. For the purpose of the simulations we exploit the second order linear system proposed by Friston et al. (Friston et al., 2000) to model the dynamic relationship between the normalised CBF and the stimulation parameters:

$$\ddot{f} + \frac{\dot{f}}{\tau_s} + \frac{(f-1)}{\tau_f} = \varepsilon u \tag{17}$$

where $\tau_s$ and $\tau_f$ are two parameters related to the dynamic characteristics of the model, and $\varepsilon$ is related to the steady state gain of the model. The input $u$ represents the stimulus, and the normalised CBF $f$ has an initial condition of 1. This model will be used to generate the normalised CBF in our simulation.

Furthermore in this paper we do not deal with the model linking deoxy-hemoglobin to the BOLD signal obtained during an fMRI experiment. Clearly the three-compartment model described in this paper will impact on the modeling and the interpretation of the BOLD signal, as the BOLD signal itself originates from a mixed compartment although previously has been largely treated as coming from only the venous compartment ((Ogawa et al., 1993), (Davis et al., 1998), (Obata et al., 2004)). By partitioning the deoxy-hemoglobin (Hbr) into arterial, capillary and venous compartments, it is possible to establish a BOLD model which reflects the different vascular sizes in the different compartments, leading to a better understanding of the importance of the different compartments to the generation of the BOLD signal. This is the work for a paper in preparation.

## MATERIALS AND METHODS

### Parameter settings

The following parameters were used in both simulation and experimental data analysis.

Total baseline saturation $S_{tot0}$. The total baseline saturation of the mixed compartment was assumed 0.5. This baseline parameter was varied between 0.4 and 0.6 when fitting the experimental data (see the discussion section), and was found to have no significant effect on the model parameter estimates.

The parameter $r_a$. The steady state ratio of the change in fractional arterial blood volume to total blood volume ($r_a$) was found by (Lee et al., 2001) to be 2.5. Using this in partitioning the CBV changes yielded an arterial blood volume change of more than 15% during the dynamic phase for a total CBV change of 5%. This arterial volume change seemed to be high compared to the average value obtained using two-dimensional OIS measurements (Berwick et al., 2004). In our simulations we set this parameter to different values to investigate its effect on the dynamics of the Hbr changes. Our observation was that $r_a = 1.5$ seemed to provide a reasonable dynamic behaviour for the arterial blood volume change as well as good predictions for the normalised Hbr.

Capillary compartment parameters. The baseline OEF was set at 0.5. The tissue oxygen concentration is modelled via the state variable $g$ which is defined as the ratio of the tissue oxygen tension to the oxygen tension at the arterial end of the capillary. According to the literature ((Hudetz, 1999), (Mintun et al., 2001), (Valabregue et al., 2003)), for a capillary permeability-surface area product (PS) of $7020 \, \text{m}\ell.\text{min}^{-1}(100\text{g})^{-1}$, the tissue oxygen tension is between 5~15mmHg. From the oxygen dissociation curve, at an arterial saturation of around 0.8, the oxygen tension is likely to be around 50mmHg. The baseline for $g$ was thus chosen as $g_0 = 0.2$. The value of $g_0$ was varied between 0.1 and 0.3 for the analysis of the experimental data sets. No significant difference in the prediction residuals was found within this parameter range.

The parameter associated with the time constant of the mean capillary oxygen concentration ($\varphi$) was set at $\varphi = 0.1$.

Venous compartment parameters. For both the 3C and 1C model, the transit time for the venous compartment was set at $\tau_v = 0.3s$.

Arterial saturation $S_a$. The 3C model presented here assumes that arterial saturation is constant. It is important to note that the following relationship exists between the total baseline saturation $S_{tot0}$ and the arterial saturation $S_a$, the baseline OEF $E_0$ and the baseline tissue oxygen concentration $g_0$:

$$S_{tot0} = p_a S_a + p_c \left( -\frac{S_a E_0}{\ln\left(1 - \frac{E_0}{1 - g_0}\right)} + S_a g_0 \right) + p_v S_a (1 - E_0) \qquad (18)$$

for given baseline blood volume proportions ($p_a, p_c, p_v$). This implies that the arterial saturation is not a free parameter once the parameters $S_{tot0}$, $E_0$, $g_0$ and ($p_a, p_c, p_v$) are selected.

A summary of the relevant parameter settings are shown in Table 2. For the 1C model simulation, $f_{tot}$ is the normalised flow into the venous compartment and $v_{tot} = v_v$. For the 3C model, the optimisation procedure described in the previous section was performed to partition $v_{tot}$ into the arterial and the venous compartments, yielding the optimal parameters for $\alpha_a$, $\beta_v$ and $\tau_{\kappa_v}$.

The normalised CBF, CBV and the metabolic demand time series generated by simulation are shown in Figure 1(a). The CBV time series is further partitioned into the arterial and the venous components, shown in Figure 1(b). Note that with a total CBV change just above 4%, the arterial blood volume change is about 10%, and the venous blood volume change is around 3%.

**Simulation data**

As a major difference between the 1C and the 3C models is the assumptions made about the arterial blood volume and saturation, simulations were used to explore the effect of the changes in these variables on the dynamics of the deoxy-hemoglobin (Hbr) downstream, in particular in the venous compartment. The results from the simulation would enable us to identify those variables which may significantly affect the shape of the deoxy-hemoglobin, and hence the BOLD signal. We will describe here the data generation process.

The normalised CBF $f_{tot}$ simulating the measured CBF was generated using a linear second order system Eqn.(17) with stimulus input being a unit pulse of 1s duration. The two parameters and the gain of the second order system were: $\tau_s = 1.0\,\text{s}$, $\tau_f = 1.11\,\text{s}$ and $\varepsilon = 0.4$ respectively. The normalised CBV $v_{tot}$ was simulated by treating the mixed compartment as one single compartment with compliance, hence the dynamic relationship governing $f_{tot}$ and $v_{tot}$ was the same as that for the venous compartment (Eqn.(7)). The parameters required were (i) the two time constants for the normalised volume and compliance state variables, set at $0.3s$ and $3.3s$ respectively; (ii) the

23

Grubb's exponent $1/\alpha$, set at $1/3$; and (iii) the exponent $\beta$ related to the delayed compliance state variable, set at $\beta = 1.7$. The above parameters were chosen based on our previous work on modelling the delayed compliance (Kong et al., 2004).

The nonlinear coupling between CBF and the metabolic demand requires a large increase in CBF for a small change in metabolic demand (Buxton and Frank, 1997). As our simulated CBF had a change of 20%, and our baseline OEF was 0.5, the magnitude of the changes in the metabolic demand was chosen as 5% (from Figure 3 of (Zheng et al., 2002)).

The parameter $\rho$ is related to the tissue oxygen concentration and was set to $\rho = 0.8$ in our simulation.

**Experimental data**

Two experimental data sets of hemodynamic changes were used. One data set was obtained using a short stimulus protocol (2s), the other from experiments using long duration stimulus protocol (20s). Both data sets were previously published ((Martindale et al., 2003), (Jones et al., 2002)) with detailed description of the experimental procedures. The methods are reviewed briefly below.

*Animal preparation*

Hooded Lister rats weighing between 250 and 400g were anaesthetised and placed in a stereotaxic holder (Kopf Instruments). A midline incision was made to expose the surface

24

of the skull. After the barrel area was marked, the skull overlying the barrels was thinned to translucency with a dental drill under constant cooling with saline. Following surgical preparation the animal was left for at least 30 min before the experiment began. The animal's rectal temperature, heart rate, breathing and blood pressure were all monitored appropriately.

*Optical imaging spectroscopy and laser Doppler flowmetry*

Both experiments collected OIS and LDF data concurrently with the stimulus being electrical stimulation of the whisker pad via tungsten electrodes. After the location of a whisker barrel cortex, the spectrograph was mounted on the CCD camera and positioned such that the $100\,\mu m$ wide slit was sited appropriately over the centre of the barrel region. This was then followed by the placement of an LDF probe ((Jones et al., 2002), (Martindale et al., 2003)). The recorded signal from the LDF probe was processed, which included a second order Butterworth lowpass filter with a bandwidth of 12kHz and a time constant of 0.2s for noise reduction purpose. This filter produced a small time lag on the recorded CBF measurements. This lag was corrected by a simple deconvolution algorithm applied to all LDF data used in this paper.

The signals from the LDF were sampled at 15Hz. The OIS data were sampled at 7.5Hz and analyzed using a pathlength scaling algorithm (Mayhew et al., 1998). To obtain fractional changes from the OIS data, the baseline total hemoglobin concentration in tissue was assumed to be $100\,\mu M$ with a saturation of 0.5 (Mayhew et al., 2000). Note that under the assumption of constant hematocrit (the percentage by volume of red blood

cells in blood), the normalised changes for total CBV is equal to the normalised changes for total hemoglobin concentration. Although there was evidence of changes in hematocrit following direct cortical electrical stimulation at high intensities (Schulte et al., 2003), at intensity ranges comparable to those used in this paper (see below), (Kleinfeld et al., 1998) found no evidence for significant changes in capillary hematocrit.

*Stimulus presentation and paradigms*

The electrical stimulation of the whisker pad was controlled through a constant-current source stimulator to generate 0.3ms pulses, with stimulus onset timing locked to the CCD camera's clock signal.

Brief stimulation: frequency modulation protocol (n=6). This data set is adapted from Martindale et al. (Martindale et al., 2003). A brief 2s stimuli of 1, 2, 3, 4 or 5Hz were randomly interleaved and applied within a single experimental run with stimulus intensity of 1.2mA and with an interstimulus interval of 25s. Thirty trials were obtained and averaged for each stimulus condition. For each trial data collection was over the period from 8s before to 15s after the stimulus onset.

Extended stimulation: intensity modulation protocol (n=7). The data set presented here is adapted from Jones et al. (Jones et al., 2002). A stimulus frequency of 5Hz was used throughout the experiment with four levels of intensity (0.4, 0.8, 1.2 and 1.6mA). The stimulus duration was 20s. Fifteen trials were obtained and averaged for each stimulus

condition, with inter-stimulus interval of 55s. For each trial, data collection started 10s before the onset of the stimulus, and it lasted for 50s.

*Parameter optimisation*

In contrast to the simulations, in which flow changes were generated using Friston's second order system linking stimulation to flow, in these studies experimentally measured flow was used directly as input to the 3C as well as the 1C models.

The models were fitted to the experimental data sets for brief and extended electrical stimulation described above, and their performance compared. Clearly there are more parameters in the 3C model which can be utilised to produce a better fit. It is therefore important that the two models are compared under similar baseline conditions. The assumption used in the OIS data analysis was that the baseline saturation was 0.5; this assumption was kept for both models. Also kept the same were the values of the baseline OEF ($E_0$), the tissue baseline oxygen concentration ($g_0$), the venous transit time ($\tau_v$) and the parameter $\varphi$ in the capillary compartment. The values of these parameters are the same as that used in the simulation studies, as shown in Table 2.

For both models, the optimisation procedure took two stages. The first stage was to use the measured normalised CBF ($f_{tot}$) to predict the normalised CBV ($v_{tot}$), hence yielding optimal parameters in the models relating CBF to CBV. For the 3C model, this was done by minimising the cost function given by Eqn.(16) above to find optimal parameters $\alpha_a$, $\beta_v$ and $\tau_{\kappa_v}$. For the 1C model which was equivalent to a venous compartment model

($v_{tot} = v_v$), this was done by optimising the parameters $\alpha_v$, $\beta_v$ and $\tau_{\kappa_v}$ to minimise the cost function:

$$L_2(\alpha_v, \beta_v, \tau_{\kappa_v}) = \sum (v_v - \hat{v}_v)^2 \tag{19}$$

where

$$\tau_v \dot{\hat{v}}_v = f_{tot} - \frac{\hat{v}_v^{\alpha_v + \beta_v}}{\kappa_v}$$

$$\tau_{\kappa_v} \dot{\kappa}_v = \hat{v}_v^{\beta_v} - \kappa_v$$

The second stage was to optimise parameters in the capillary compartment to predict the total normalised Hbr ($q_{tot}$). We chose to optimise the following two parameters for both models: (i) The magnitude of the metabolic demand $K_M$. This would provide us with useful information about the coupling between CBF and the metabolic demand. (ii) The parameter $\rho$ related to the time constant of tissue oxygen concentration. This is a lumped parameter with a scaling factor introduced in Zheng et al. (Zheng et al., 2002). The value of this parameter affects the speed of response to the tissue oxygen concentration. The existing literature does not provide a value for this parameter hence we attempt to estimate it through the model.

Thus the parameters $K_M$ and $\rho$ are optimised by minimising the following cost function

$$L_3(K_M, \rho) = \sum (q_{tot} - \hat{q}_{tot})^2 \tag{20}$$

All optimisation algorithms were implemented in Matlab™ (The MathWork, Inc, Cambridge) using the built-in function *lsqnonlin* utilising the Levenberg-Marquardt method.

# RESULTS

## Simulations

Simulated CBF and CBV data were analysed using the 3C model while manipulating the parameters which distinguished the 3C and 1C models. These parameters were: (i) baseline CBV proportions; (ii) fractional CBV changes in the arterial, and hence the venous compartments; (iii) arterial oxygen saturation ($S_a$). The objective of the simulation study was to investigate how these parameters may affect the dynamics of the deoxy-hemoglobin (Hbr) in the venous compartment in order to determine how this would affect the BOLD signal predicted by current biophysical models.

The dynamics of normalised Hbr are moderately affected by baseline CBV proportions. While keeping $S_{tot0}$ and $E_0$ unchanged, we varied the proportions $p_a$, $p_c$ and $p_v$ of the baseline CBV in the three compartments and compared the normalised Hbr time courses in the venous compartment ($q_v$). We first kept $p_a = 25\%$ and varied $p_c$ within the range $5\% \le p_c \le 25\%$. It was observed that at smaller capillary volume fractions, the initial increase in $q_v$ was small, followed by a large decrease due to increases in CBF which washes away Hbr and replaces with $HbO_2$, resulting in increases in oxygen supply in response to increased metabolic demand. As $p_c$ increases, the initial increase in $q_v$ was more obvious, and the subsequent decrease in $q_v$ was smaller (Figure 2a). We then varied $p_a$ in the range $15\% \le p_a \le 35\%$ while keeping $p_c$ constant at $15\%$. The initial

increase in $q_v$ was less obvious at smaller arterial volume fractions. The effect of changing $p_a$ on the subsequent decrease in $q_v$ was only slight, as shown in Figure 2b.

Note that changes in the baseline CBV proportions, while keeping $S_{tot0}$ and $E_0$ unchanged, implies changes in the baseline arterial saturation $S_a$. For the range of values used here, the arterial saturation baseline varied only slightly from 0.73 to 0.79.

The dynamics of normalised Hbr are markedly affected by fractional arterial CBV changes. As discussed above, the choice of $r_a$ determines the amount of fractional CBV changes in the arterial compartment, and hence the venous compartment. We selected three different values for $r_a$ (0.5, 1.5, 2.5), thus generating three time courses for the fractional arterial CBV changes, shown in Figure 3(a). The corresponding dynamics of $q_v$ are notably different, shown in Figure 3(b). For $r_a = 0.5$, there is an obvious initial increase in $q_v$, followed by a larger decrease. As $r_a$ becomes larger, the initial rise in $q_v$ becomes less visible. At $r_a = 2.5$, $q_v$ decreases almost immediately after the onset of stimulus. At this value of $r_a$, it is impossible to find a plausible set of parameter values that produce an initial increase in $q_v$. This suggests that the initial dip in the BOLD signal is less likely to occur for proportionally large arterial CBV increases.

The percentage decrease in normalised Hbr is affected by arterial oxygen saturation. We varied the arterial saturation $S_a$ to three different levels (0.7, 0.8, 0.9). Note that while keeping the baseline OEF constant at $E_0 = 0.5$, this implies that the total baseline

30

saturation $S_{tot0}$ will change accordingly (Eqn.(18)). The normalised Hbr in the venous compartment was shown in Figure (4) from which we observe that increasing arterial saturation from 0.7 to 0.9 has the effect of increasing venous Hbr changes from 3.5% (at $S_a = 0.7$) to 7% (at $S_a = 0.9$). This is as expected because higher arterial oxygen saturation implies more oxygen supply for the same fractional changes in CBF. Note that as the arterial saturation is assumed constant, the normalised deoxy-hemoglobin in the arterial compartment $q_a$ is the same as $v_a$, hence its time course is not affected by changes in the arterial oxygen saturation.

**Experimental data**

Under each experimental condition described in the previous section, we fitted the 1C and 3C models to the CBF, CBV and Hbr data which were averaged over animals. Two data sets are shown in this paper for display purposes, one from each protocol. The data set for short stimulation protocol has a stimulus frequency of 5Hz and a intensity of 1.2mA. For the extended stimulation, the data selected has the same stimulus frequency of 5Hz, but with a stimulus intensity of 1.6mA.

*Optimisation to fit the normalised CBV*

There is no significant difference between the two models for the first stage of the optimisation. As can be seen in Figure 5 the predicted CBV time series for both models is an excellent fit to the data.

For the 1C model, the optimised parameters are: $\alpha_v = 2.9$ (corresponding to a Grubb's exponent of 0.34), $\beta_v = 1.6$ and $\tau_c = 3.4$ s. For the 3C model, the optimised parameters are: for the arterial compartment, $\alpha_a = 2.0$ (corresponding to a Grubb's exponent of 0.5); for the venous compartment: $\beta_v = 4.1$ and $\tau_{\kappa_v} = 2.0$ s. The parameter $\alpha_v$ is calculated from Eqn.(15) as $\alpha_v = 2.9$ (corresponding to a Grubb's exponent of 0.34). The similarity of the fit of the CBV data for both models ensures that if there is any difference between the two models in the goodness-of-fit to the normalised Hbr data, it cannot be attributed to any mismatch in the time series of the changes in blood volume.

*Optimisation to fit the normalised Hbr*

Figure 6 shows representative results from each of the experimental paradigms. The optimisation results clearly demonstrate that the 3C model fits the experimental data better than the 1C model. One characteristic of the predicted changes in Hbr using the 1C model is a much bigger initial increase in the predicted normalised Hbr than that measured. A lower value for the parameter representing the metabolic demand would improve the initial fit to the Hbr data but at the expense of a much larger decrease later in the response than that measured. In the case of the 3C model, there is no such problem. An explanation of this difference between the models may be that because in the 1C model arterial saturation is assumed to be 100%, for corresponding flow increases there is a greater delivery of oxygenated blood than in the case of the 3C model.

Tables 3(a) and 3(b) show the optimised model parameters under all stimulus conditions for both models. The last column in each Table shows the F-ratio calculated with the

numerator being the variance of the prediction error using the 1C model, and the denominator being that using the 3C model. From the two Tables, we make the following observations.

(i)      The estimated metabolic demand for the 1C model is generally much larger than that for the 3C model.

(ii)     The estimated metabolic demand for the 1C model consistently increases with increases in intensity and frequency of stimulation. However, because of the very poor fit to the Hbr time series data (see Figure 6) we do not believe this can be supported.

(iii)    For the 3C model under extended stimulation, the metabolic demand seems to increase with increased stimulus intensity, except at intensity of 1.2mA where the model parameters are outside the normal range. Looking at the data closely, we found that the normalised Hbr has a dominant undershoot after the stimulus onset before it increases to a steady state plateau. But this feature was not present in either CBF or CBV. We believe that the model attempted to fit this undershoot by reducing the metabolic demand to the hard limit of zero set in the optimisation algorithm.

(iv)    For the 3C model under brief stimulation conditions, there was no trend in the changes in metabolic demand with respect to changes in frequency.

(v)     The F-ratios under all conditions indicate that the prediction errors obtained using the 3C model are significantly better than those obtained using the 1C model at $p \leq 0.05$ taking appropriate account of the degrees of freedom for the two models.

33

# DISCUSSION

In this paper we have introduced a three-compartment hemodynamic model which relates the normalised time series of Hbr to neural activity induced changes in CBF. The main novel characteristics of the model are: (i) arterial baseline blood volume is included in the calculation of the changes in the normalised CBV, and significantly, arterial CBV changes with changes in CBF; (ii) arterial saturation can be less than unity; (iii) capillary CBV is also involved in the calculation but remains constant, i.e., there is no capillary recruitment or dilation.

The effects of the above on the dynamics of the changes in deoxy-hemoglobin in the venous compartment ($q_v$) showed that:

(i)     The baseline CBV proportions within a sensible range had moderate effect on the dynamics (i.e., the shape of the time course) of $q_v$.

(ii)    The fractional CBV changes in the arterial compartment contributed significantly to the dynamics of $q_v$. For small arterial fractional CBV changes, a prominent initial increase in $q_v$ could be observed. This initial increase disappeared as the arterial fractional CBV changes increased. Thus the amount of fractional arterial CBV changes could be one of the influencing factors to the presence or otherwise of the initial dip in the BOLD signal.

(iii)   A lower arterial saturation baseline decreased the magnitude of the reduction in Hbr in the venous compartments.

34

The model was also tested on experimental OIS data and the model parameters were optimised to give the best fit to the measured deoxy-hemoglobin data in the least squares manner. The results were compared with that of the one-compartment model (Zheng et al., 2002). Two parameters were optimised: the metabolic demand and the tissue time constant. The 3C model produced significantly better fit to the data than the 1C model.

**Tissue oxygen tension**

The time course of the state variable $g$ represents the time variation in tissue oxygen tension. Although this quantity was not measured, it was predicted by both models as a state variable. Figures 7(a) and 7(b) compare the predictions of $g$ for both models under the brief and extended stimulation respectively. It can be seen that over the duration of the stimulus application, the predicted tissue oxygen tension decreases. Once stimulation ceased, tissue oxygen tension increases and overshoots its baseline before returning to it. This holds true over all experimental conditions examined. However the difference between the 1C and 3C models is the degree to which the tissue tension changes. For the 1C model, the predicted value of $g$ decreased significantly more than that predicted by the 3C model, but the overshoot when returning to baseline was much smaller in the 1C compared to that of the 3C model.

Preliminary comparison between these time series and the measured tissue oxygenation time series published by Thompson et al. (Thompson et al., 2003) were made for the brief stimulation paradigm, and we found that the time courses of $g$ predicted by the 3C

model resemble their measurements much more closely than those of the 1C model. Further research and a more comprehensive study will be needed in this area.

**Capillary permeability-surface area product.**

As the 3C model is an extension of the previous 1C model (Zheng et al., 2002), many of the assumptions made there are also implicit here. One such assumption is that oxygen diffuses from capillaries into the tissue at a rate proportional to the oxygen tension difference between plasma and tissue. Another assumption is that the nonlinear Hill equation relating the blood oxygen concentration in the capillary ($C_B$) to that in plasma ($C_P$) can be satisfactorily approximated by a linear relationship $C_P = rC_B$ ((Buxton and Frank, 1997), also see the Appendix B of (Zheng et al., 2002)) where $r$ is a constant. These assumptions lead to the result that the oxygen concentration along the capillary decays exponentially, making it possible to study the transport of oxygen in simpler terms than using the nonlinear Hill equation (Valabregue et al., 2003).

The appropriateness of the linear assumption above depends on the choice of the capillary permeability-surface area product (PS) and that of the CBF baseline. Kassissia et al. (Kassissia et al., 1995) studied the cerebral micro-circulation of awake animals (n=5) and found that the CBF range was $70.8 \pm 18.6\,\text{(SD)}\ \text{m}\ell.\text{min}^{-1}(100\text{g})^{-1}$, and that for PS the range was $7020 \pm 1020\,\text{(SD)}\ \text{m}\ell.\text{min}^{-1}(100\text{g})^{-1}$. Valabreque et al. (Valabregue et al., 2003) pointed out that if the capillary permeability-surface area product is significantly different from the above value (e.g., they used PS=3600 $\text{m}\ell.\text{min}^{-1}(100\text{g})^{-1}$) and that CBF varies through a wide range such as from 50 to 200 $\text{m}\ell.\text{min}^{-1}(100\text{g})^{-1}$, then

36

the exponential approximation may not adequately describe the oxygen transfer process between the capillary compartment and its surrounding tissue.

Figures 8 and 9 compare the results obtained using the Hill's equation with those using the exponential decay model. These figures were produced assuming zero tissue oxygen tension and tetramer haemoglobin concentration of $2.3 mmol.l^{-1}$, the same as those used in (Valabregue et al., 2003). In Figure 8, the parameter $r = C_P/C_B$ is the decay coefficient used in the exponential decay model. It is varied between 0.0076 and 0.0094 while PS is kept constant at $7020 m\ell.min^{-1}(100g)^{-1}$. It can be seen that for both of the relationships between CBF and OEF (Figure 8(a)), and $CMRO_2$ (Figure 8(b)), the curves produced by the Hill's equation can be well approximated by the exponential decay model at $r = 0.0082$, provided the blood flow is within the range 50 to 100 $m\ell.min^{-1}(100g)^{-1}$. Figure 9 compares the relationships between the normalised $CMRO_2$ and the normalised CBF obtained using the Hill's equation and the exponential decay model for different values of PS. The baseline CBF is kept constant at 66 $m\ell.min^{-1}(100g)^{-1}$. Again the exponential decay model at PS = $7020 m\ell.min^{-1}(100g)^{-1}$ coincides well with the solution produced via the Hill's equation for CBF change of up to 30%. For all the data presented in this paper, the change in CBF is around or below 30%, hence we are satisfied that the assumption of exponential decay for oxygen concentration along the capillaries is appropriate for our study.

**Changes in the assumed baseline oxygen saturation and total hemoglobin concentration for OIS data.**

The OIS data sets were converted to the form of fractional changes using the assumed baseline hemoglobin values: a hemoglobin concentration (Hbt) of 100μM and saturation of 0.5. We selected, arbitrarily, a data set (brief stimulation at 4Hz) to test how sensitive our model fits are to the above baseline assumptions.

First the total oxygen saturation baseline was changed to 0.4 and 0.6, and the optimisation procedure was repeated. It was observed that both changes resulted in poorer model fit compared with that for $S_{tot0} = 0.5$.

The assumption of Hbt baseline of 100μM has been recognised as being slightly higher than the generally accepted value (Appendix I). Hence this value was lowered to 75μM and 50μM. The OIS data were re-calculated and the model parameters were optimised. It was observed that the 3C model is able to fit the modified data without any significant changes to the prediction error variances. The main difference is in the estimation of metabolic demand which decreases with decreasing baseline Hbt values, from 5.2% at Hbt baseline of 100μM to 4.1% and 2.1% at Hbt baselines of 75μM and 50μM respectively. This may be explained by the fact that lower Hbt baseline leads to an increase in the fractional CBV changes. This will in turn increase slightly the fractional changes in Hbr, i.e., making it more negative. Without any increase to the normalised CBF, the larger negative fractional change in Hbr can only be accounted for by reducing the metabolic demand.

38

**Choice of optimisation parameters**

We have demonstrated that the 3C model was able to fit the optical imaging spectroscopy data much better than the 1C model. The prediction errors for the 3C model were significantly less than for the 1C model. Although it is true that the 3C model has more parameters to manipulate than the 1C model, the number of parameters we chose to optimise was the same for both models, and the other parameters in the two models were matched wherever possible. We based our choice of the parameters to be optimised largely on the uncertainty in the literature about the physiological ranges of these parameters, and that the parameter values assigned via optimisation may provide us with some useful information.

It was noted that some of the model parameters are highly related, i.e., the effect of changing one parameter on the output of the model can be very similar to that of changing another parameter. A preliminary study of the sensitivity of the 3C model to parameter variations was conducted and a more detailed analysis will be carried out which may provide a useful insight to the selection of the parameters that most affect the dynamics of the model output.

**CONCLUSION**

We have shown in this paper that both the 1C and 3C model were able to fit the time series of the change in volume very well, however the important finding was that when the fitted parameters values were then used to fit the times series of the changes in Hbr,

the 3C model far outperformed the 1C model. This really is not surprising because the 1C model makes the unrealistic simplifying physiological assumption that the volume and saturation measurements derive from a single compartment of the microvasculature, specifically the venous compartment. This assumption, commonplace in previous work (e.g. (Hoge et al., 1999), (Buxton and Frank, 1997), (Mandeville et al., 1999b), (Hyder et al., 1998), (Friston et al., 2000)) applied to the modelling and interpretation of the BOLD signal from low field strength human experiments is unsafe if, as seems to be the case that, the BOLD signal derives from a mixture of intra- and extra-vascular effects arising in both the capillary and venous compartments of the microvasculature. Furthermore the work of Lee et al. (Lee et al., 2001), which clearly implicates the arterial compartment of the microvasculature in the blood volume changes, underlines the importance of the development of the three-compartment biophysical model of the hemodynamic response, not only of the BOLD signal but also for the interpretation of the CBV-MRI (e.g. (Mandeville et al., 1999a), (Wu et al., 2002)) and perfusion data (Detre et al., 1992) in the studies of functional activation.

The development of an appropriate and physiologically plausible hemodynamic model is crucial for the interpretation of the BOLD signals, in that the model can be used to recover the underlying changes in neural activity. We think that the three-compartment model provided an important basis for such development.

## Appendix I. Calculation of the hemoglobin concentration in brain tissue

Most text books present hemoglobin concentration in blood in the unit grams per litre (or decilitre). This appendix outlines the procedure for converting this value to the hemoglobin concentration in brain tissue in the unit μM. The selected physiological parameter values only serve as examples to the conversion process.

The hemoglobin concentration in blood refers to the amount of hemoglobin (in grams) per unit blood volume (in litres). The normal hemoglobin range is species dependent and is also dependent on the age and gender. The range for human adult male is 135-175g/$\ell$. For illustration purpose, we will use a value of 150g/$\ell$ as the hemoglobin concentration.

The hemoglobin concentration in blood decreases with the vessel size; the figure of 150g/$\ell$ is for a blood sample taken from large vessels. The cerebral-to-large vessel hematocrit ratio measures the decrease in concentration as blood flows into the brain, and is 0.69 (Wyatt et al., 1990). Thus the hemoglobin concentration in blood in the cerebral regions of the brain can be found as 150×0.69 = 103.5g/$\ell$.

To convert the above into the hemoglobin concentration in brain tissue, we need to know the ratio of the cerebral blood volume to tissue volume. The average cerebral blood volume concentration in tissue is $3.3(\pm0.4)\times10^{-5}\ell$/g (Hamberg et al., 1996) and the cerebral tissue density is around $1.05\times10^{3}$ g/$\ell$ (Sabatini et al., 1991). Thus the blood-to-

tissue volume ratio in percentages can be calculated as: $(3.3 \times 10^{-5}) \times (1.05 \times 10^{3}) \times 100 = 3.47\%$.

This gives us the hemoglobin concentration in cerebral tissue as $103.5 \times 0.0347 = 3.6g/\ell$. The generally preferred unit for hemoglobin concentration is mol/$\ell$ (also known as Molar, denoted by M). By using the molecular weight of hemoglobin which is 64450 g/mol, the hemoglobin concentration in g/$\ell$ can be converted into mol/$\ell$ as $3.6/64450 = 56 \times 10^{-6} mol/\ell = 56$ µmol/$\ell = 56$µM.

This suggests that the assumption of 100µM for the hemoglobin concentration in brain tissue is higher than the normal expectation for this value.

We emphasise again that the above value of 56µM is dependent on the other physiological parameters used during the conversion. These parameters vary depending on species, age and gender among other factors. Hence the above value of hemoglobin concentration in brain tissue only serves as a guideline.

42

## ACKNOWLEDGEMENTS

## REFERENCES

Aubert, A., and Costalat, R. 2002. A model of the coupling between brain electrical activity, metabolism, and hemodynamics: application to the interpretation of functional neuroimaging. *Neuroimage* **17:** 1162-1181.

Berwick, J., Johnston, D., Jones, M., Martindale, A. J., and Mayhew, J. E. W. 2004. Exploitation of 2D optical imaging spectroscopy to investigate the hemodynamic response in different vascular compartments. *Program No. 642.14. 2004 Abstract Viewer/Itinerary Planner, Washington, DC: Society for Neuroscience 2004.*

Buxton, R. B., and Frank, L. R. 1997. A model for the coupling between cerebral blood flow and oxygen metabolism during neural stimulation. *J Cereb Blood Flow Metab* **17:** 64-72.

Buxton, R. B., Wong, E. C., and Frank, L. R. 1998. Dynamics of blood flow and oxygenation changes during brain activation: the balloon model. *Magn Reson Med* **39:** 855-864.

Davis, T. L., Kwong, K. K., Weisskoff, R. M., and Rosen, B. R. 1998. Calibrated functional MRI: mapping the dynamics of oxidative metabolism. *Proc Natl Acad Sci U S A* **95:** 1834-1839.

Detre, J. A., Leigh, J. S., Williams, D. S., and Koretsky, A. P. 1992. Perfusion imaging. *Magn Reson Med* **23:** 37-45.

Duong, T. Q., and Kim, S. G. 2000. In vivo MR measurements of regional arterial and venous blood volume fractions in intact rat brain. *Magn Reson Med* **43:** 393-402.

Friston, K. J., Mechelli, A., Turner, R., and Price, C. J. 2000. Nonlinear responses in fMRI: the Balloon model, Volterra kernels, and other hemodynamics. *Neuroimage* **12:** 466-477.

Gjedde, A., Poulsen, P. H., and Ostergaard, L. 1999. On the oxygenation of hemoglobin in the human brain. *Adv Exp Med Biol* **471:** 67-81.

Grubb, R. L., Jr., Raichle, M. E., Eichling, J. O., and Ter-Pogossian, M. M. 1974. The effects of changes in PaCO2 on cerebral blood volume, blood flow, and vascular mean transit time. *Stroke* **5:** 630-639.

Hamberg, L. M., Hunter, G. J., Kierstead, D., Lo, E. H., Gilberto Gonzalez, R., and Wolf, G. L. 1996. Measurement of cerebral blood volume with subtraction three-dimensional functional CT. *AJNR Am J Neuroradiol* **17:** 1861-1869.

Hathout, G. M., Varjavand, B., and Gopi, R. K. 1999. The early response in fMRI: a modeling approach. *Magn Reson Med* **41:** 550-554.

Hayashi, T., Watabe, H., Kudomi, N., Kim, K. M., Enmi, J., Hayashida, K., and Iida, H. 2003. A theoretical model of oxygen delivery and metabolism for physiologic interpretation of quantitative cerebral blood flow and metabolic rate of oxygen. *J Cereb Blood Flow Metab* **23:** 1314-1323.

Hoge, R. D., Atkinson, J., Gill, B., Crelier, G. R., Marrett, S., and Pike, G. B. 1999. Investigation of BOLD signal dependence on cerebral blood flow and oxygen consumption: the deoxyhemoglobin dilution model. *Magn Reson Med* **42:** 849-863.

Hudetz, A. G. 1999. Mathematical model of oxygen transport in the cerebral cortex. *Brain Res* **817:** 75-83.

Hyder, F., Shulman, R. G., and Rothman, D. L. 1998. A model for the regulation of cerebral oxygen delivery. *J Appl Physiol* **85:** 554-564.

Jones, M., Berwick, J., and Mayhew, J. 2002. Changes in blood flow, oxygenation, and volume following extended stimulation of rodent barrel cortex. *Neuroimage* **15:** 474-487.

Kassissia, I. G., Goresky, C. A., Rose, C. P., Schwab, A. J., Simard, A., Huet, P. M., and Bach, G. G. 1995. Tracer oxygen distribution is barrier-limited in the cerebral microcirculation. *Circ Res* **77:** 1201-1211.

Kleinfeld, D., Mitra, P. P., Helmchen, F., and Denk, W. 1998. Fluctuations and stimulus-induced changes in blood flow observed in individual capillaries in layers 2 through 4 of rat neocortex. *Proc Natl Acad Sci U S A* **95:** 15741-15746.

Kong, Y., Zheng, Y., Johnston, D., Martindale, J., Jones, M., Billings, S., and Mayhew, J. 2004. A model of the dynamic relationship between blood flow and volume changes during brain activation. *J Cereb Blood Flow Metab* **24:** 1382-1392.

Lee, S. P., Duong, T. Q., Yang, G., Iadecola, C., and Kim, S. G. 2001. Relative changes of cerebral arterial and venous blood volumes during increased cerebral blood flow: implications for BOLD fMRI. *Magn Reson Med* **45:** 791-800.

Mandeville, J. B., Marota, J. J., Ayata, C., Moskowitz, M. A., Weisskoff, R. M., and Rosen, B. R. 1999a. MRI measurement of the temporal evolution of relative $CMRO_2$ during rat forepaw stimulation. *Magn Reson Med* **42:** 944-951.

Mandeville, J. B., Marota, J. J., Ayata, C., Zaharchuk, G., Moskowitz, M. A., Rosen, B. R., and Weisskoff, R. M. 1999b. Evidence of a cerebrovascular postarteriole windkessel with delayed compliance. *J Cereb Blood Flow Metab* **19:** 679-689.

Martindale, J., Mayhew, J., Berwick, J., Jones, M., Martin, C., Johnston, D., Redgrave, P., and Zheng, Y. 2003. The hemodynamic impulse response to a single neural event. *J Cereb Blood Flow Metab* **23:** 546-555.

Mayhew, J., Hu, D., Zheng, Y., Askew, S., Hou, Y., Berwick, J., Coffey, P. J., and Brown, N. 1998. An evaluation of linear model analysis techniques for processing images of microcirculation activity. *Neuroimage* **7:** 49-71.

Mayhew, J., Johnston, D., Berwick, J., Jones, M., Coffey, P., and Zheng, Y. 2000. Spectroscopic analysis of neural activity in brain: increased oxygen consumption following activation of barrel cortex. *Neuroimage* **12:** 664-675.

Mintun, M. A., Lundstrom, B. N., Snyder, A. Z., Vlassenko, A. G., Shulman, G. L., and Raichle, M. E. 2001. Blood flow and oxygen delivery to human brain during functional activity: theoretical modeling and experimental data. *Proc Natl Acad Sci U S A* **98:** 6859-6864.

Obata, T., Liu, T. T., Miller, K. L., Luh, W. M., Wong, E. C., Frank, L. R., and Buxton, R. B. 2004. Discrepancies between BOLD and flow dynamics in primary and supplementary motor areas: application of the balloon model to the interpretation of BOLD transients. *Neuroimage* **21**: 144-153.

Ogawa, S., Menon, R. S., Tank, D. W., Kim, S. G., Merkle, H., Ellermann, J. M., and Ugurbil, K. 1993. Functional brain mapping by blood oxygenation level-dependent contrast magnetic resonance imaging. A comparison of signal characteristics with a biophysical model. *Biophys J* **64**: 803-812.

Sabatini, U., Celsis, P., Viallard, G., Rascol, A., and Marc-Vergnes, J. P. 1991. Quantitative assessment of cerebral blood volume by single-photon emission computed tomography. *Stroke* **22**: 324-330.

Schulte, M. L., Wood, J. D., and Hudetz, A. G. 2003. Cortical electrical stimulation alters erythrocyte perfusion pattern in the cerebral capillary network of the rat. *Brain Res* **963**: 81-92.

Thompson, J. K., Peterson, M. R., and Freeman, R. D. 2003. Single-neuron activity and tissue oxygenation in the cerebral cortex. *Science* **299**: 1070-1072.

Vafaee, M. S., and Gjedde, A. 2000. Model of blood-brain transfer of oxygen explains nonlinear flow-metabolism coupling during stimulation of visual cortex. *J Cereb Blood Flow Metab* **20:** 747-754.

Valabregue, R., Aubert, A., Burger, J., Bittoun, J., and Costalat, R. 2003. Relation between cerebral blood flow and metabolism explained by a model of oxygen exchange. *J Cereb Blood Flow Metab* **23:** 536-545.

Vovenko, E. 1999. Distribution of oxygen tension on the surface of arterioles, capillaries and venules of brain cortex and in tissue in normoxia: an experimental study on rats. *Pflugers Arch* **437:** 617-623.

Wu, G., Luo, F., Li, Z., Zhao, X., and Li, S. J. 2002. Transient relationships among BOLD, CBV, and CBF changes in rat brain as detected by functional MRI. *Magn Reson Med* **48:** 987-993.

Wyatt, J. S., Cope, M., Delpy, D. T., Richardson, C. E., Edwards, A. D., Wray, S., and Reynolds, E. O. 1990. Quantitation of cerebral blood volume in human infants by near-infrared spectroscopy. *J Appl Physiol* **68:** 1086-1091.

Zheng, Y., Martindale, J., Johnston, D., Jones, M., Berwick, J., and Mayhew, J. 2002. A model of the hemodynamic response and oxygen delivery to brain. *Neuroimage* **16:** 617-637.

## Figure legends

Figure 1. The time series generated for the simulations. (a) The simulated flow (solid), volume (dotted) and metabolic demand (dashed) were used in the first stage of optimisation. (b) The partitioning of the volume (solid) into the arterial (dotted) and venous (dashed) parts is one of the results of the first stage of optimisation and is principally determined by $r_a$. Stimulus duration is 1s.

Figure 2. Changes in the normalised Hbr in the venous compartment for different CBV baseline proportions. (a) With $p_a$ fixed at 25%, $p_c$ was set to 5%, 15% and 25%, and $p_v$ was varied accordingly. (b) With $p_c$ fixed at 15%, $p_a$ was set to 15%, 25% and 35%, and $p_v$ was varied accordingly.

Figure 3. (a) The fractional arterial to total volume ratio $r_a$ directly affects the arterial volume change. (b) This leads to indirect effects downstream such as increasing the initial 'bump' in the venous Hbr as $r_a$ is decreased.

Figure 4. Effect of changing the arterial saturation $S_a$ on the normalised Hbr in the venous compartment.

Figure 5. Predictions of the normalised CBV using the 1C model and the 3C model, superimposed with the normalised CBV data for (a) brief stimulation (5Hz, 1.2mA) and (b) extended stimulation (5Hz, 1.6mA). They are both excellent.

Figure 6. Predictions of the normalised Hbr using the 1C model and the 3C model, compared to the normalised Hbr data for (a) brief stimulation (5Hz, 1.2mA) and (b) extended stimulation (5Hz, 1.6mA). There are obvious shortcomings in the 1C model whilst the 3C model captures virtually all the dynamics of the system.

Figure 7. Predictions of the state variable $g$ using the 1C model and the 3C model for (a) brief stimulation (5Hz, 1.2mA) and (b) extended stimulation (5Hz, 1.6mA).

Figure 8. Comparison of the solutions using the Hill equation (solid curves with plus signs) with those using the exponential decay model at a range of values of the decay coefficient $r$ for PS=7020m$\ell$.min$^{-1}$.(100g)$^{-1}$. Note that the Hill equation can be well approximated by exponential model over CBF=50~100m$\ell$.min$^{-1}$.(100g)$^{-1}$ for $r = 0.0082$.

Figure 9. Comparison of the CMRO$_2$ calculations using the Hill equation (solid lines) and the exponential decay model (dotted lines) at different capillary permeability-surface area product PS for the baseline CBF of 66m$\ell$.min$^{-1}$.(100g)$^{-1}$. At PS=7020m$\ell$.min$^{-1}$.(100g)$^{-1}$, the curve obtained using the exponential decay model fits well to that obtained via the Hill equation.

Figure 1

Figure 2.

(a)

(b)
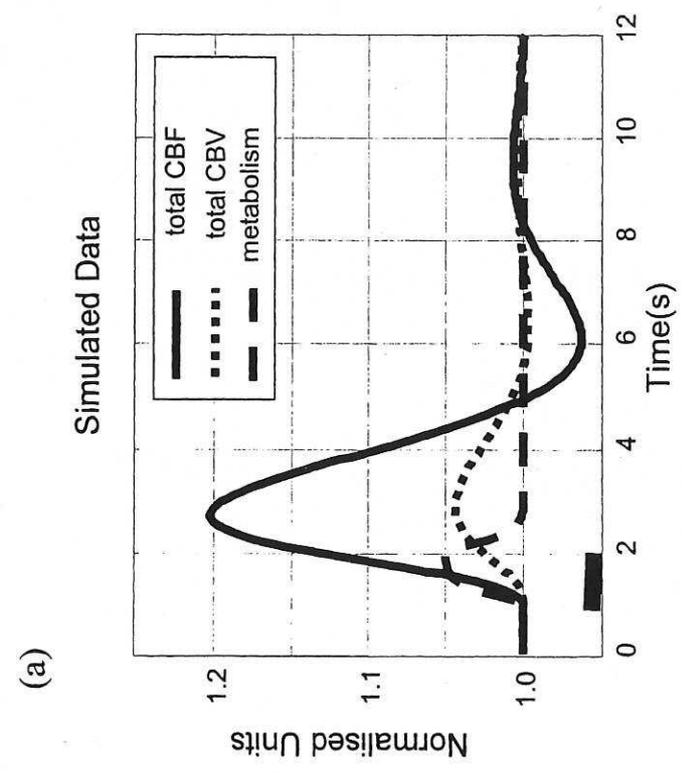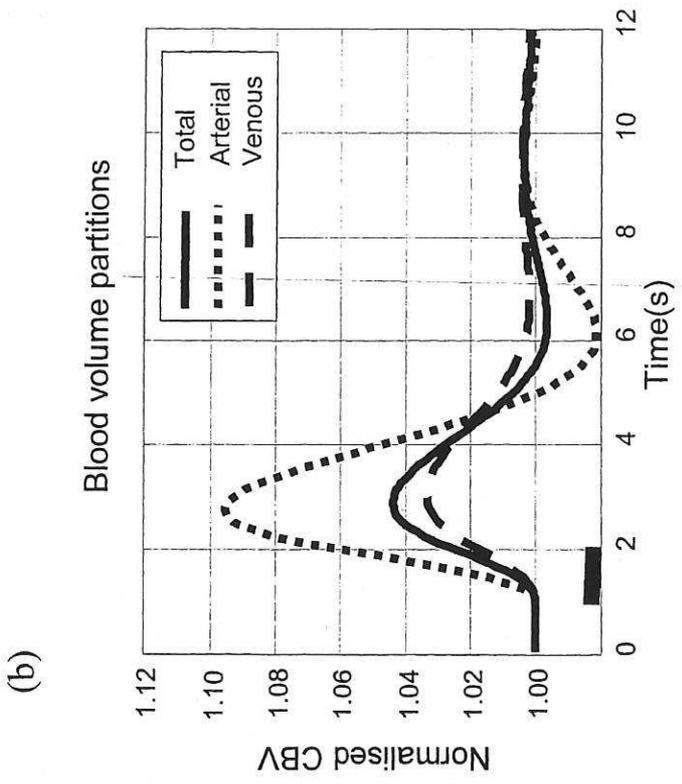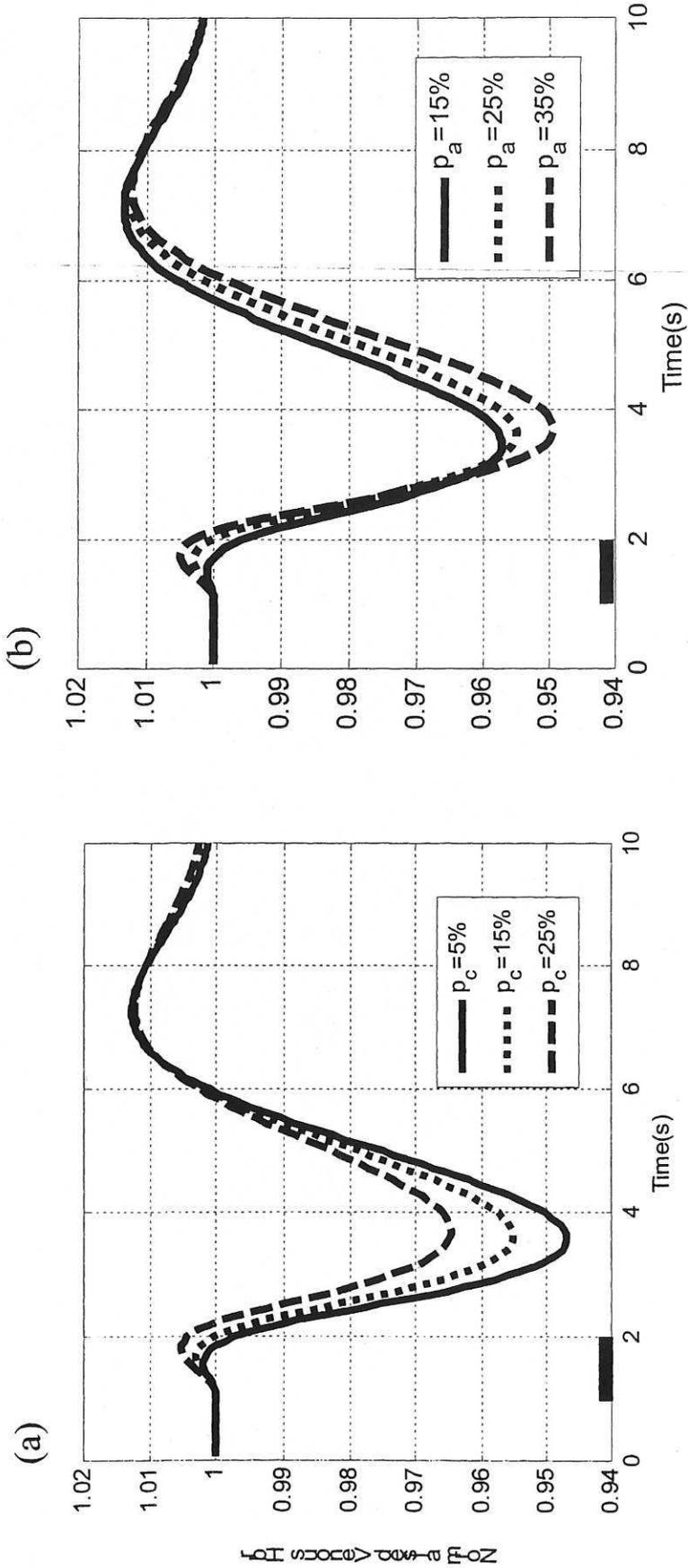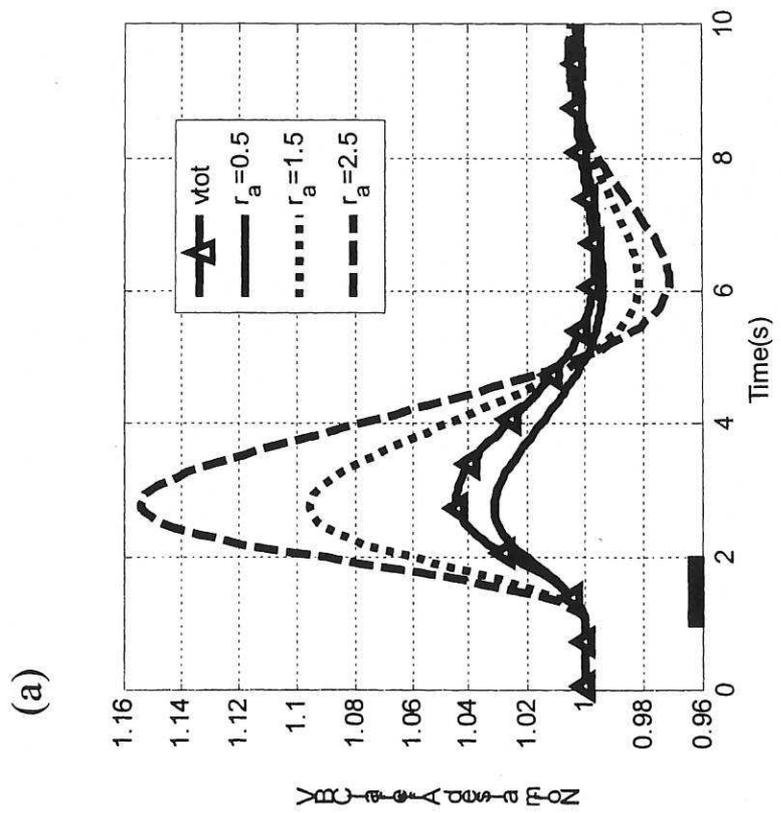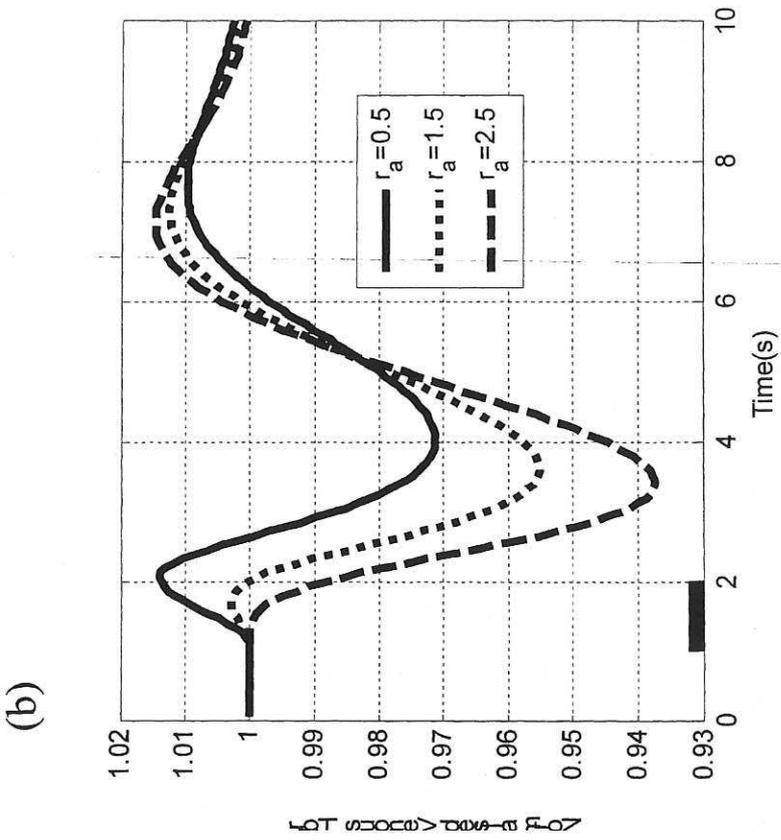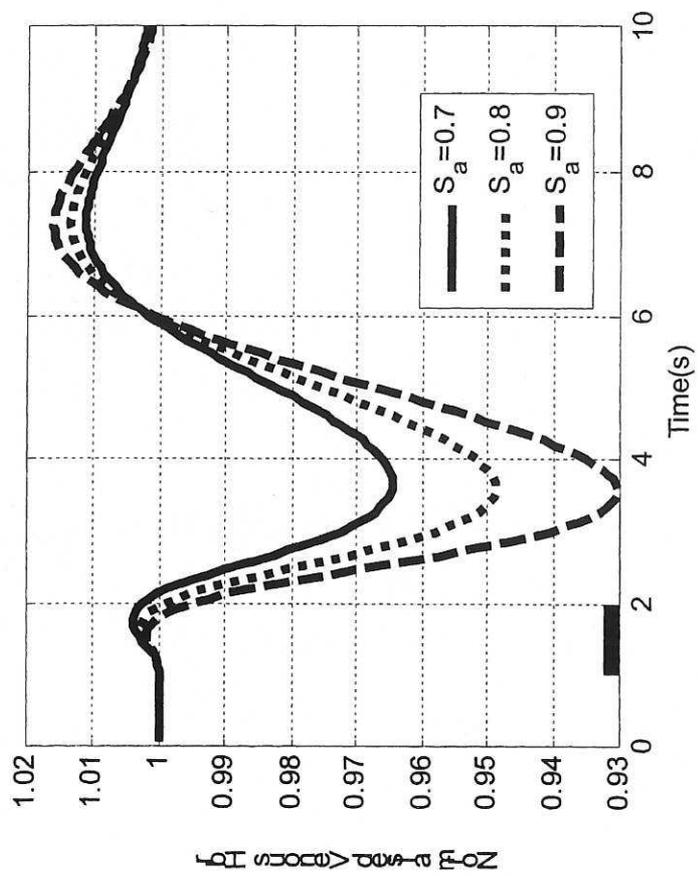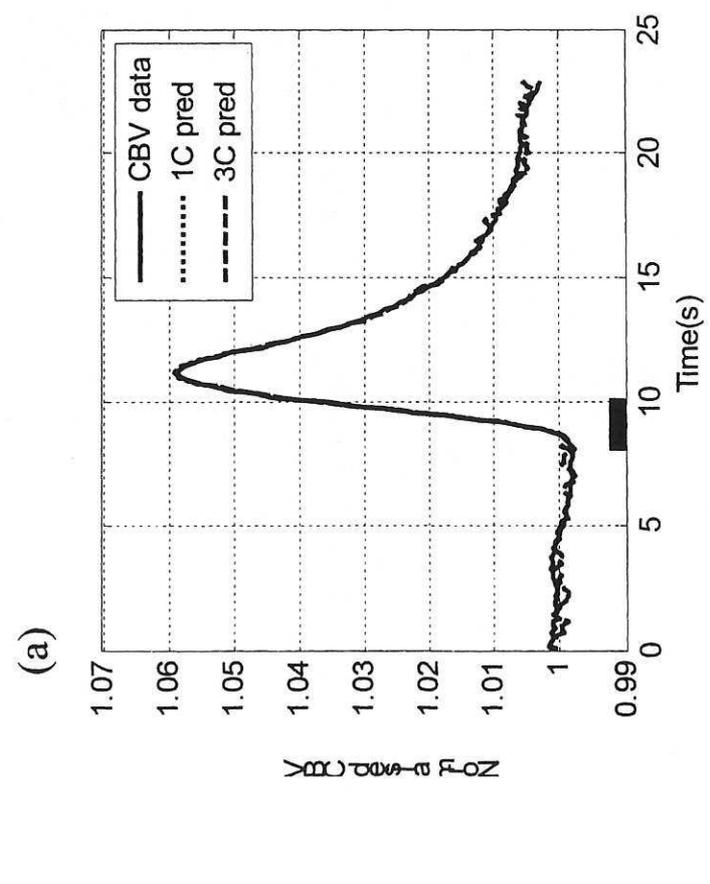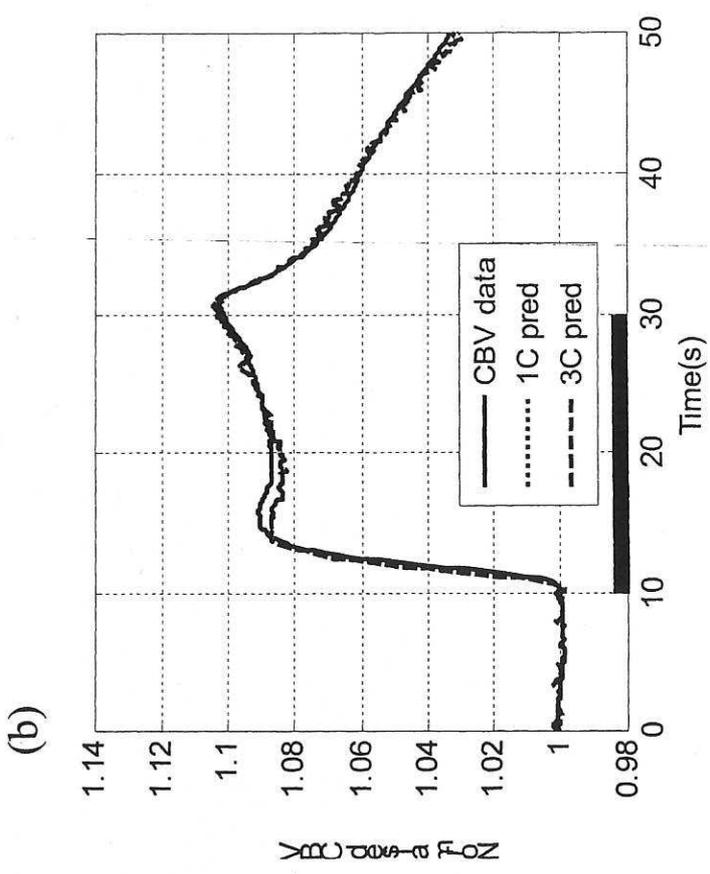
Figure 3

Figure 4

Figure 5

Figure 6

Figure 7

(a)

(b)
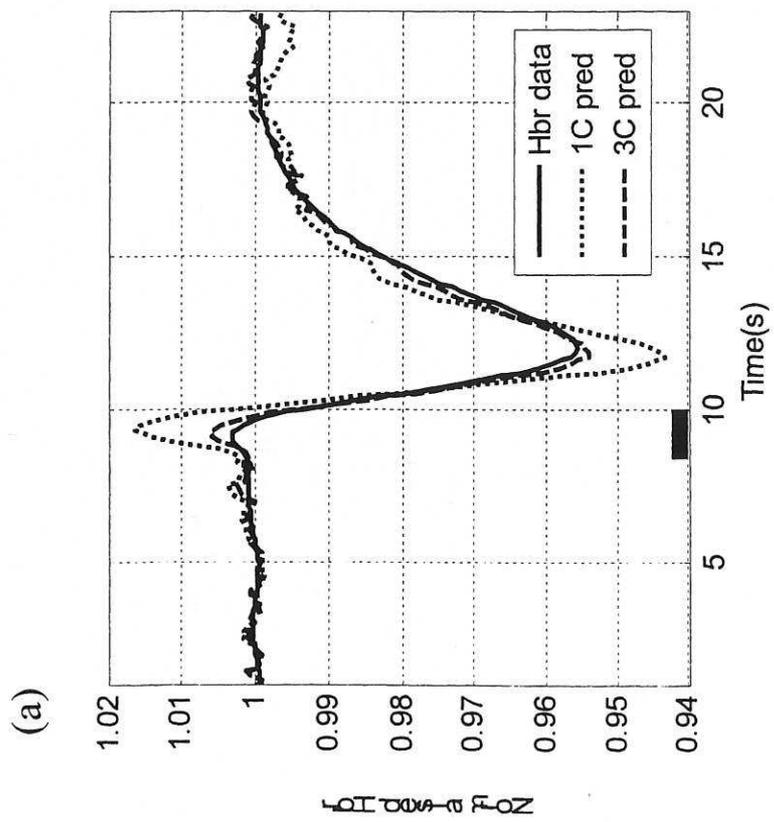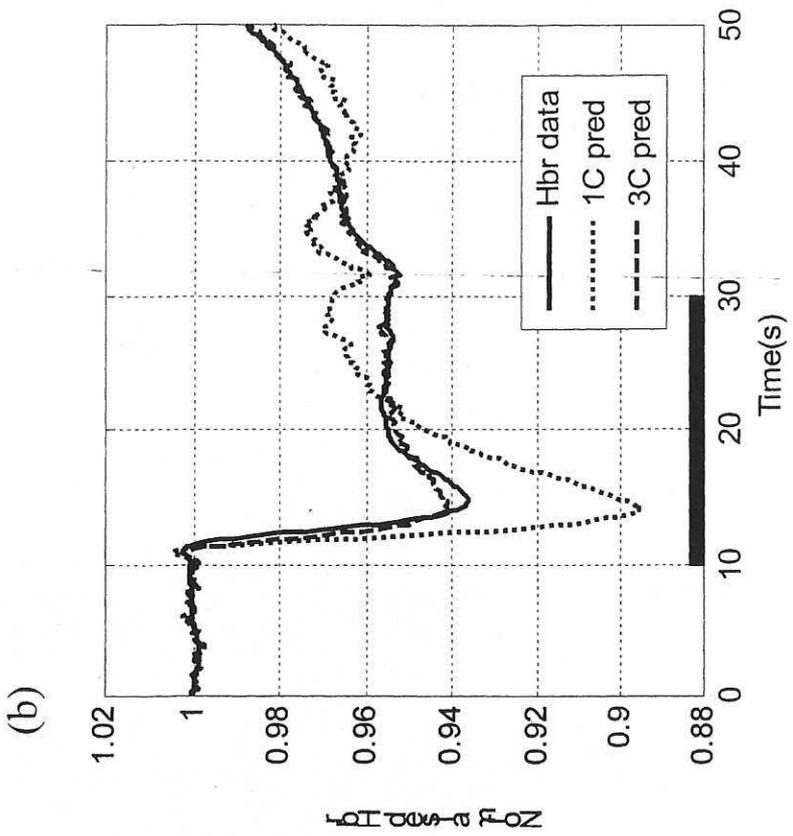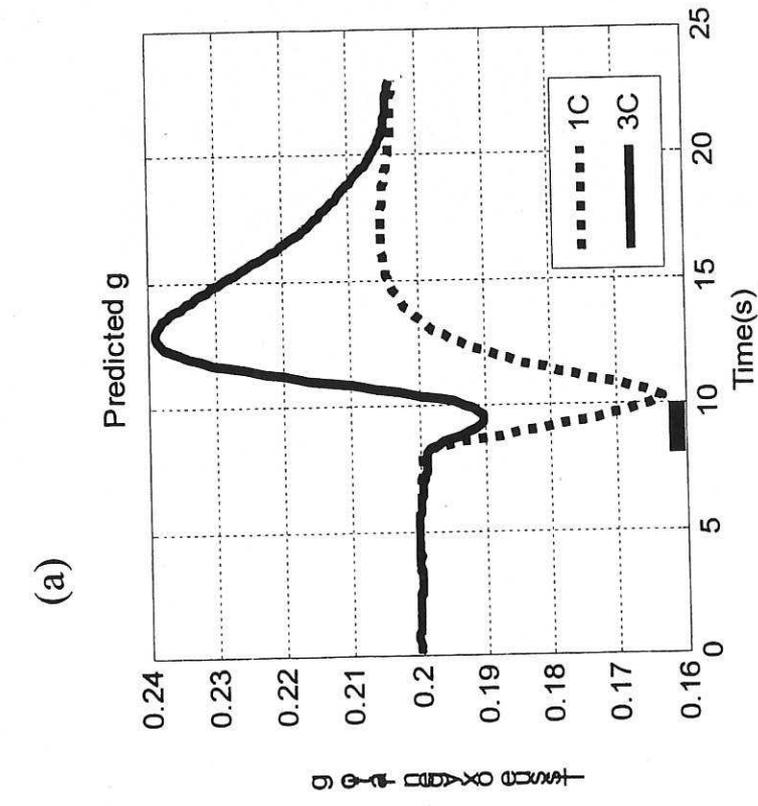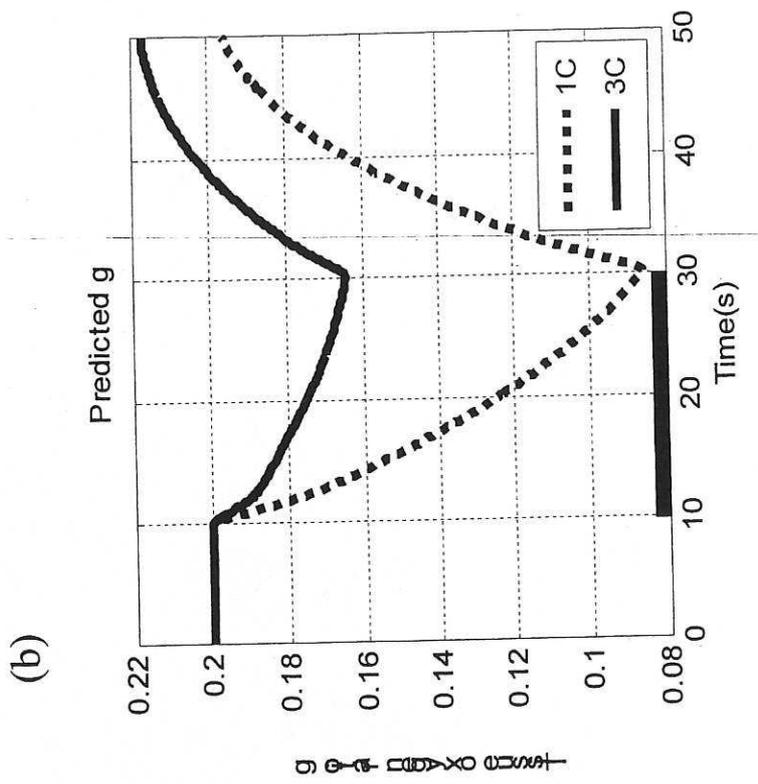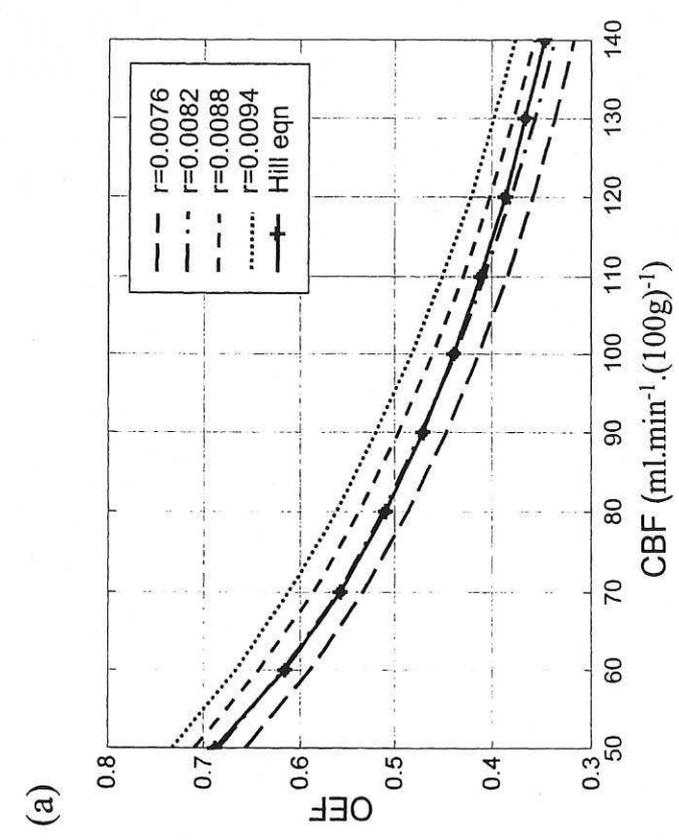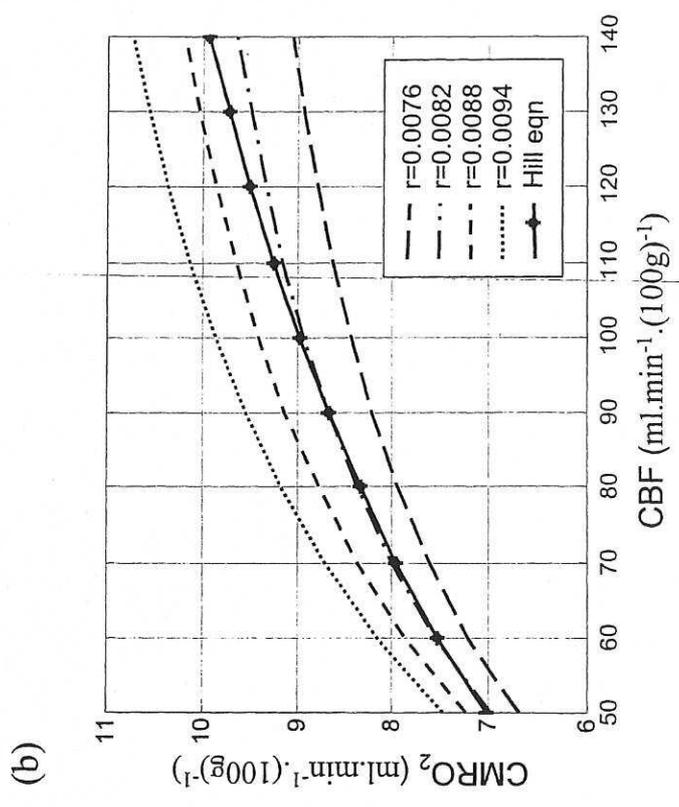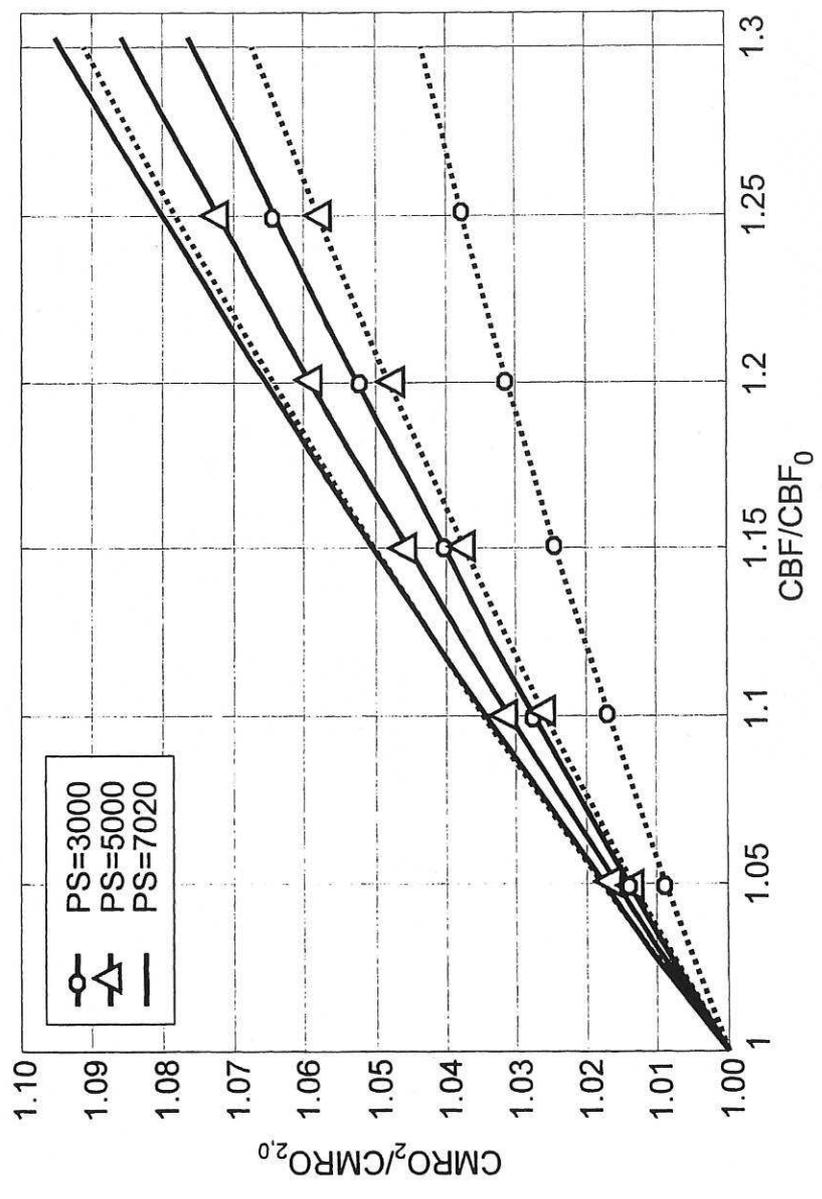
Figure 8

Figure 9

Table 1. Three-compartment partitioning.

| Flow partitions | $f_{tot} = w_a f_{a,in} + w_c f_c + w_v f_{v,out}$ <br><br> $w_a + w_c + w_v = 1$ |
|---|---|
| Baseline volume partitions | $V_{tot0} = V_{a0} + V_{c0} + V_{v0}$ <br><br> $\dfrac{V_{a0}}{V_{tot0}} = p_a, \quad \dfrac{V_{c0}}{V_{tot0}} = p_c, \quad \dfrac{V_{v0}}{V_{tot0}} = p_v,$ <br><br> $p_a + p_c + p_v = 1$ |
| Volume change partitions | $\Delta V_{tot} = \Delta V_a + \Delta V_v$ <br><br> $\dfrac{\Delta V_a}{V_{a0}} \cong r_a \dfrac{\Delta V_{tot}}{V_{tot0}}, \quad \dfrac{\Delta V_v}{V_{v0}} \cong r_v \dfrac{\Delta V_{tot}}{V_{tot0}}, \quad p_a r_a + p_v r_v = 1$ |
| Normalised volume partitions | $v_{tot} = p_a v_a + p_c v_c + p_v v_v, \qquad v_c = 1$ |
| Saturation partitions | $S_{tot} = \dfrac{p_a v_a}{v_{tot}} S_a + \dfrac{p_c v_c}{v_{tot}} \bar{S}_c + \dfrac{p_v v_v}{v_{tot}} S_v$ |
| Deoxy-hemoglobin partitions | $q_{tot} = v_{tot} \dfrac{1 - S_{tot}}{1 - S_{tot0}}$ <br><br> $= \dfrac{p_a(1 - S_a)}{1 - S_{tot0}} q_a + \dfrac{p_c(1 - \bar{S}_{c0})}{1 - S_{tot0}} \bar{q}_c + \dfrac{p_v(1 - S_{v0})}{1 - S_{tot0}} q_v$ |

Table 2. Parameters used in the simulation of the three-compartment model.

| Global model parameters | Symbol | Value |
|---|---|---|
| Total baseline oxygen saturation | $S_{tot0}$ | 0.5 |
| Weighting coefficients for CBF | $w_a : w_c : w_v$ | 0.33 : 0.33 : 0.33 |
| Baseline volume proportions | $p_a : p_c : p_v$ | 0.25 : 0.15 : 0.6 |
| Ratio of normalised changes in arterial CBV to total CBV | $r_a$ | 1.5 |
| Magnitude of the metabolic demand | $K_M$ | 5% |
| **Parameters for the arterial compartment** | | |
| Arterial compartment transit time (s) | $\tau_a$ | 0.2 |
| **Parameters for the capillary compartment** | | |
| Parameter related to capillary transit time | $\varphi$ | 0.1 |
| Parameter related to time constant of $g$ | $\rho$ | 0.8 |
| Baseline oxygen extraction fraction | $E_0$ | 0.5 |
| Baseline tissue to arterial oxygen concentration ratio | $g_0$ | 0.2 |
| **Parameters for the venous compartment** | | |
| Venous compartment transit time (s) | $\tau_v$ | 0.3 |

Table 3a. Brief stimulation.

| Stimulus frequency | 1-compartment | | 3-compartment | | F-ratio |
|---|---|---|---|---|---|
| | $\rho$ | Metab (%) | $\rho$ | Metab (%) | |
| 1Hz | 3.36 | 8.7 | 17.8 | 3.8 | 2.1 |
| 2Hz | 2.95 | 9.6 | 1.33 | 2.8 | 4.4 |
| 3Hz | 3.03 | 11.7 | 1.60 | 1.1 | 16.6 |
| 4Hz | 3.19 | 19.6 | 0.95 | 5.2 | 7.6 |
| 5Hz | 3.70 | 19.5 | 1.28 | 0.92 | 13.4 |

Table 3b. Extended stimulation.

| Stimulus intensity | 1-compartment | | 3-compartment | | F-ratio |
|---|---|---|---|---|---|
| | $\rho$ | Metab (%) | $\rho$ | Metab (%) | |
| 0.4mA | 7.8 | 3.0 | 56.1 | 4.0 | 5.3 |
| 0.8mA | 9.5 | 12.0 | 38.5 | 9.4 | 15.4 |
| 1.2mA | 11.2 | 23.5 | 137 | 0 | 32.4 |
| 1.6mA | 13.2 | 38.2 | 17.2 | 21.8 | 26.0 |